# Artificial Intelligence supported road vehicle suspension design

DOCTOR THESIS

Yansong Huang

Department of Mechanics and Maritime Sciences Chalmers University of Technology Gothenburg, Sweden, 2025

### Artificial Intelligence supported road vehicle suspension design DOCTOR THESIS

Yansong Huang ISBN 978-91-8103-237-6

Acknowledgements, dedications, and similar personal statements in this thesis, reflect the author's own views.

© Yansong Huang 2025 except where otherwise stated.

Selected material from the author's licentiate thesis: Yansong Huang, "Target-driven road vehicle suspension design", *CHALMERS*, Gothenburg, Sweden, Dec. 2022, is republished in this Ph.D. thesis.

Doktorsavhandlingar vid Chalmers tekniska högskola Ny serie nr5695 ISSN  $0346\text{-}718\mathrm{X}$ 

Department of Mechanics and Maritime Sciences Chalmers University of Technology SE-412 96 Gothenburg, Sweden Phone: +46 (0)31 772 1000

Printed by Chalmers Digital Printing Gothenburg, Sweden, August 2025

#### Artificial Intelligence supported road vehicle suspension design

DOCTOR THESIS
YANSONG HUANG
Department of Mechanics and Maritime Sciences
Chalmers University of Technology

#### **Abstract**

This thesis presents an AI-supported framework for vehicle suspension design, combining reinforcement learning (RL) and reverse engineering to automate hardpoint optimization. A case study demonstrates a 50% reduction in design lead time. The proposed framework uses RL to derive suspension kinematics targets from vehicle-level requirements and reverse engineering to convert these targets into hardpoint configurations. The full case study demonstrates the practical application of this integrated methodology. The findings conclude that AI-supported suspension design algorithms significantly enhance both the efficiency and precision of suspension architecture development.

The wheel suspension represents one of the most architecture-intensive systems in automotive design, largely determining a vehicle's motion characteristics and performance boundaries. Increasing pressures from electrification and intensifying global competition demand accelerated and more efficient development of new vehicle concepts, even within traditional domains like mechanical wheel suspension design. This system encompasses numerous design parameters with intricate interdependencies. Conventionally, development relies heavily on highly specialized engineering expertise. A significant bottleneck in modern suspension development involves balancing complex performance requirements that currently require time-consuming iterations. Today's development process also involves virtual subjective assessment alongside traditional chassis engineering experience. Addressing these challenges requires a full review of the entire development workflow—from initial target setting through verification and subsequent optimization loops.

**Keywords:** Kinematics, compliance, suspension, reverse design, reinforcement learning, target

#### List of Publications

This thesis is based on the following publications:

- [A] **Huang, Y.**, Brandin, T., Jacobson, B., "Linear and Nonlinear Kinematic Design of Multilink Suspension". SAE Int. J. Passeng. Veh. System,vol 16(2) (2023).
- [B] Naik, A., Brandin, T., **Huang, Y.** et al., "Target Driven Bushing Design for Wheel Suspension Concept Development". SAE Technical Paper 2023-01-0638 (2023).
- [C] **Huang, Y.**, Johannes, K., et al., "Optimized Rear-Axle Concept for Battery Electric Vehicles". 6th Shanghai-stuttgart-symposium automotive and powertrain technology.
- [D] Köpler, J., **Huang, Y.** et al., "Automated Methods for the suspension pre-development Design of a front axle for a long range electric vehicle". Chassis.tech plus 2023 Munich, Germany.
- [E] **Huang, Y.**, Boerboom, M. et al., "Find optimal Suspension kinematics targets using reinforcement learning". Submitted to Journal on Aug. 13th 2025.

and patent applications:

[F] Molin D., Sellergren M., Brandin T., and Huang Y., "Table rear wheel steering geometry for Integral rear suspension". *Chinese patent application no. CN114633594A*, 2022.

#### Contents

ΑI	bstrac	ct		i
Li	st of	Papers		iii
Αd	cknov	/ledgen	nents	ix
Αd	crony	ms		x
I	O۱	/ervie\	N	1
1	Intr	oductio	on	3
	1.1	Backg	round and motivation	3
		1.1.1	Traditional development process with V-model	5
		1.1.2	Finding optimal suspension kinematics targets using re-	
			inforcement learning	6
		1.1.3	Target-driven road vehicle suspension design	7
	1.2	Resear	rch question	8
	1.3	Theor	y, methods and limitations	9
		1.3.1	Theory and method	9
	1.4	Thesis	s outline and contribution	11
		1.4.1	Scientific contributions	12

		1.4.2	Organizational and societal contributions	16
2	Met	hod		17
	2.1	Kinen	natics and compliance	17
		2.1.1	Model	17
		2.1.2	Target identification	25
		2.1.3	Target-driven reverse design method	31
	2.2	Targe	t setup using RL	37
		2.2.1	Simulation environment	37
		2.2.2	Learning agent	40
3	Case	e study	,	45
	3.1	•	lete vehicle target setup	47
	3.2	_	arning process	50
	3.3		ing curve for suspension targets	52
	3.4		nsion target representation (KDT Target)	55
	3.5	Hardp	point setup (KDT Suspension)	58
	3.6	Closin	ig the design loop	58
	3.7	Summ	nary	62
4	Con	clusion		63
	4.1	Summ	nary of research contributions	63
	4.2		icance and impact	64
		4.2.1	Efficiency enhancements	64
		4.2.2	Cross-functional collaboration	65
		4.2.3	Improved design quality	65
		4.2.4	Balance between AI and human expertise	66
		4.2.5	Holistic system understanding	67
	4.3	Limita	ations and future research directions	67
		4.3.1	Scope expansion	68
		4.3.2	Integration of compliance and kinematics	68
		4.3.3	Nonlinear compliance behavior	69
		4.3.4	Transfer learning and knowledge reuse	69
	4.4	Concl	uding remarks	70
Re	eferer	ices		73

II Papers	79
Paper A	83
Paper B	99
Paper C	115
Paper D	131
Paper E	153

#### **Acknowledgments**

I would like to express my profound gratitude to my industrial supervisor, Tobias Brandin, for initiating this project and providing invaluable guidance throughout the research journey. His expertise and insights have significantly elevated the quality of this work. It has been a privilege to work and study under his mentorship. I am also deeply indebted to the suspension architecture team at Volvo Cars. Special thanks to my manager, Jenny Berglund, for her administrative support, and to my colleagues Akshay Naik, Max Boerboom, and Daniel Molin for their generous assistance and collaboration.

At Chalmers University of Technology, I extend my sincere appreciation to my academic supervisors, Professor Bengt Jacobson and Associate Professor Krister Wolff, for their insightful supervision and thought-provoking questions. I am grateful to Sonja for her efficient handling of administrative matters, and to my examiner, Professor Mattias Wahde, for his valuable guidance. The supervision group from the Research Institute for Automotive Engineering and Powertrain Systems Stuttgart (FKFS) has provided exceptional learning opportunities and fostered excellent collaboration. I particularly thank Dr. Jens Neubeck from FKFS for his supervision and administrative support. I am also indebted to my colleagues Johannes Köpler and Ambrosoli Pascal for our enriching technical and non-technical discussions.

This thesis would not have been possible without the financial support from VINNOVA through the Fordonsstrategisk forskning och innovation (FFI) program.

Finally, my deepest gratitude goes to my family for their unwavering encouragement, endless support, and unconditional love throughout this journey.

Yansong Huang Göteborg, September 2025

#### **Acronyms**

AI: Artificial Intelligence

BEV: Battery Electric Vehicle

CAD: Computer-Aided Design

CAE: Computer-Aided Engineering

HP: Hardpoint

KDT: Kinematic Design Tool

MBS: Multi-Body System

MCP: Motion Control Point

NVH: Noise, Vibration, and Harshness

RCH: Roll Center Height

RL: Reinforcement Learning

TD: Temporal Difference

WCH: Wheel Center Height

WLLA: Wheel Load Level Arm

# Part I Overview

#### CHAPTER 1

Introduction

This chapter provides an outline of the thesis. After discussing the motivations behind the work in detail in Section 1.1, the main research questions are formulated in Section 1.2. The theory, methods, and limitations are presented in Section 1.3. Finally, the main contributions are summarized in Section 1.4.

#### 1.1 Background and motivation

The automotive industry faces growing pressure to reduce costs and development time while maintaining performance. Engineering development lead-time has been reduced to meet time-to-market targets. The Concept Development phase described by [1] is key to ensuring products meet market demands. Suspension concept development is a cross-functional process addressing multiple attribute targets such as ride comfort, handling, steering (kinematics and compliance), packaging, styling, durability, and noise and vibration (NVH), making it time-consuming. Most of these attribute targets in concept development are tied to suspension kinematics-hardpoint development. Having quick suspension kinematics design iterations in the concept phase is therefore critical for improving efficiency throughout the entire project.

In the traditional development V-model [2], concept development and validation are two phases that ensure the end product meets targets at the complete vehicle level. The process cascades targets hierarchically: from vehicle-level to system-level, then to subsystem-level. Each level of the system has a validation phase to make sure the design meets its corresponding target, thereby ensuring the vehicle meets the complete vehicle level target. Prior work [3–6] uses simplified vehicle dynamics models to cascade system and subsystem targets efficiently. The model must balance fidelity and simplicity to accurately capture behavior while remaining tractable for optimization. The suspension kinematics target requires a medium to high complexity model to capture the influence of suspension kinematics on complete vehicle behavior. However, such a model contains a set of design parameters which might cause the searching algorithm to fail to find the solution space due to the model complexity.

Once suspension kinematics targets are successfully cascaded from complete vehicle targets, suspension design engineers face the challenge of determining optimal hardpoints that fulfill these targets. While traditional optimization methods [7–11] facilitate hardpoint adjustment to meet suspension characteristic behaviors, they present significant limitations. Particularly problematic are the difficulties in formulating optimization cost functions that adequately represent complex packaging constraints and achieve balanced performance targets. This makes traditional optimization approaches inefficient for hardpoint configuration in complex packaging environments. Moreover, achieving critical suspension compliance targets requires not only appropriate bushing specifications but also the correct hardpoint setup. Consequently, suspension kinematics, compliance, and packaging must be considered holistically to meet overall behavioral targets. This necessitates an efficient methodology capable of evaluating compliance behavior and configuring bushing compliance parameters according to specific compliance targets.

The suspension design challenges outlined above motivate this research, which is structured in two key parts. The first part aims to develop an efficient approach for cascading suspension kinematics targets from complete vehicle requirements. The second part utilizes these derived targets to systematically configure suspension hardpoints and bushing compliance parameters.

#### 1.1.1 Traditional development process with V-model

A typical passenger car development process follows a structured flow from project definition to production start. The widely adopted 'V model' effectively divides this process into concept and validation phases. Figure 1.1 illustrates the key milestones throughout this V-shaped development cycle, highlighting three hierarchical levels: complete vehicle, subsystems, and components.

The process begins with comprehensive simulations that establish targets for each hierarchical level. A method called target cascading systematically breaks down objectives from the complete vehicle level to subsystems and components. This cascading process must ensure adequate tuning margins while maintaining coherent relationships between targets across different levels. During the validation phase, both simulations and prototype vehicles are employed to evaluate subjective and objective targets, confirming that requirements are met at each level [12].

The development necessarily involves iterations between concept and validation phases, as significant system balancing and compromise constitute essential parts of the process. Consequently, development timeframes typically extend to several years, depending on customer requirements and project complexity [13, 14].

The V model facilitates effective requirement setting and verification across all development levels. To reduce development time while maintaining precision, modern automotive development increasingly relies on simulation-based cascading. For example, complete vehicle simulations determine appropriate requirements for subsystems (such as the front axle) and subsequently verify whether subsystem designs collectively deliver satisfactory vehicle performance. Similarly, subsystem-level simulations establish component requirements (for links and bushings) and verify their collective performance. Therefore, there is great potential to develop a method that can synthesize the requirements setting and verification across subsystem and component levels.

In certain design iterations, physical testing may substitute for simulations, utilizing test rigs, prototype vehicles, or driving simulators. Prototype vehicles and driving simulators offer the particular advantage of allowing assessment of subjective requirements that cannot be fully captured through simulation alone.

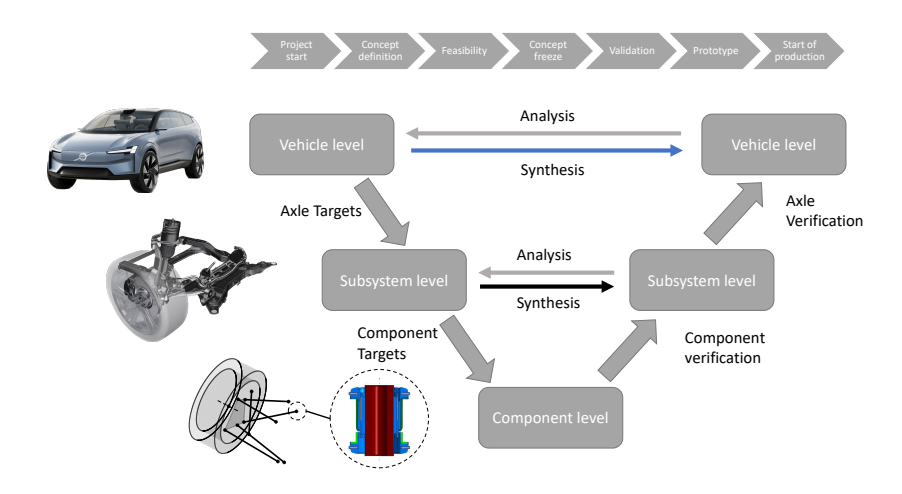


Figure 1.1. Synthesize the V development process [2, 15, 16]

# 1.1.2 Finding optimal suspension kinematics targets using reinforcement learning

Suspension kinematics targets are established based on vehicle attributes, which are determined by vehicle dynamics that are influenced by suspension kinematics and other vehicle subsystems. Traditionally, vehicle engineers set these targets using their expertise and experience. While optimization techniques [17] can transform this process into a computational task, significant challenges persist—including convergence issues, balancing exploration versus exploitation, and computational efficiency—particularly in high-dimensional design spaces [18, 19]. Expert engineers leverage accumulated knowledge from previous experiences when proposing new designs. Drawing inspiration from this human approach, neural network foundations [20, 21] enable knowledge representation through network weights that can be updated through environmental interaction. This principle forms the basis of reinforcement learning (RL), which has demonstrated remarkable effectiveness in solving complex problems [22]. This study addresses the absence of efficient optimization methods for high-dimensional suspension kinematics design by employing RL algorithm to identify optimal suspension targets.

#### 1.1.3 Target-driven road vehicle suspension design

Having established optimal suspension targets from 1.1.2, we now discuss target-based design. Current methods for verifying wheel suspension design requirements typically rely on axle-level simulations using multi-body system (MBS) software. These simulations parameterize suspension systems through springs, dampers, joint and bushing locations (hardpoints), and compliance specifications. Improvements are identified by testing various combinations of hardpoints and bushing parameters. This process often involves manual trial-and-error, making it inherently slow. While optimization techniques are sometimes employed, they are challenging to configure and remain computationally expensive due to the numerous simulations required. Additionally, optimization setup typically demands human guidance. The workflow's reliance on multiple software tools further extends development time, as information sharing between platforms consumes significant resources.

Researchers have developed various methods for calculating suspension kinematics [23–25]. Visualization techniques introduced in [26–28] enable engineers to directly calculate and analyze kinematic performance from specified hardpoints. Compliance design primarily addresses bushing elasticity, with established methods for simulating compliance behaviors [29–31]. These modeling and simulation approaches transform hardpoint configurations and bushing specifications into behavior reports, such as kinematic and compliance analyses. In vehicle development projects, axle-level targets must satisfy requirements from attribute leaders—a time-intensive process complicated by constantly evolving targets. The iterative refinement of axle design to meet these shifting targets represents a critical component of the overall vehicle development process.

This project aims to develop knowledge, methods, and tools for semiautomatically translating wheel suspension axle requirements into optimized hardpoint and bushing configurations. The resulting tool will be designed for suspension engineers, enabling an agile working framework with targetbased design capabilities and rapid adaptation to requirement changes. This approach will significantly accelerate concept selection while enhancing engineers' system understanding. Consequently, more development time can be dedicated to improving cost, quality, durability, and weight. One project objective involves quantifying both time savings and quality improvements, particularly measuring efficiency gains from requirement updates to new design proposals. The complete solution requires a comprehensive tool encompassing the entire concept suspension development process with an intuitive user interface.

#### 1.2 Research question

This research fundamentally challenges the traditional simulation paradigm by reversing the process flow from component design to performance evaluation [32]. Specifically, it aims to automatically generate suspension targets from complete vehicle requirements, and subsequently derive hardpoints and bushing specifications from these suspension targets. The reverse algorithm innovatively mimics human expert reasoning. Rather than iterating through simulations, the approach establishes direct pathways from complete vehicle targets to specific suspension requirements, and further to the precise hardpoint and bushing configurations needed to fulfill these requirements.

From a vehicle engineering perspective, this approach enables the establishment of comprehensive performance targets without immediate concern for construction details or system feasibility. Kinematically, it provides specific hardpoint design guidelines with clearly defined linear and nonlinear targets. The model accommodates additional targets, progressively constraining design freedom as needed. Regarding compliance, the research addresses how to systematically determine optimal bushing stiffness specifications to meet compliance objectives.

Beyond technical engineering contributions, this project aims to enhance the effective development of new vehicle concepts where suspension systems are integral components. The originality lies in reverse-engineering methodologies that emulate human expertise. While current AI applications (including machine learning and optimization) often focus on replacing complex simulations in verification processes, this research takes the opposite approach—identifying patterns and equations to determine optimal inputs for desired outputs. The research questions are articulated as follows:

- Can reverse methods improve suspension design efficiency while reducing lead time?
- What modeling frameworks, virtual methodologies, and requirement specifications are essential to effectively connect vehicle and suspension

design?

- How can AI methodologies optimize suspension design within the broader vehicle development process?
- What new modeling, simulation, requirement, and verification approaches are necessary when integrating AI methods?
- How can human expertise and AI collaborate optimally in suspension design?
- How can human domain knowledge effectively guide and accelerate machine learning processes?
- Which AI methodologies are most appropriate and effective for road vehicle suspension design?

#### 1.3 Theory, methods and limitations

This section provides an overview of the theories and methods presented in this thesis, along with their limitations.

#### 1.3.1 Theory and method

Papers A and B introduce a methodology that utilizes suspension kinematics and compliance targets to determine hardpoints and bushing stiffness. For suspension kinematics analysis, two precise computational approaches exist. The first method, investigated by [23], analyzes kinematics from hardpoints by formulating velocity constraints, thereby transforming specific hardpoint configurations into general motions that express suspension kinematics. Albers [24] expanded this approach to encompass broader kinematic behaviors, including suspension steering and jounce travel<sup>1</sup> maneuvers. The second method employs Jacobian differentiation for analytical calculations. Developed by Hazem [25], this approach formulates a constraints matrix through differentiation, offering a direct method to derive acceleration constraints by double-differentiating position constraints. While computationally intensive,

<sup>&</sup>lt;sup>1</sup> Jounce travel means the wheel center height change with respect to the design position - positive named as jounce, negative named as rebound.

it requires less modeling effort than the first approach. Kinematic calculations can be utilized in various ways, with visualization being crucial for interpreting performance through geometric features such as steering kingpin axes and roll centers [33, 34]. Sommer III [28] demonstrates a calculation method to visualize first and second-order instant screw features. Paper A explores novel hardpoint control methods derived from first-order linear targets and introduces additional control techniques based on higher-order targets.

The suspension compliance algorithm begins with calculating forces at various joints and bushings. Rocca [35] and Knapczyk [36] developed a linear force matrix using free-body diagrams by decomposing suspension systems into individual components, thus enabling force distribution calculation. Liang [37] enhanced this approach to incorporate bushing nonlinear elasticity by segmenting nonlinear deformation curves into smaller linear segments—an effective yet computationally intensive method as equation complexity increases with accuracy requirements. Paper B presents an efficient method for reversing compliance design based on a linearized model derived from nonlinear suspension dynamics. Kang [38] describes the linearization of steadystate suspension models using a Jacobian matrix for kinematic constraints. The combination of each bushing's stiffness matrix and the Jacobian matrix forms comprehensive force equations for calculating bushing deformation. Caputo [39] demonstrates how to identify each bushing's contribution to compliance targets, enabling engineers to optimize bushing parameters for balanced compliance performance.

Papers C and D apply these methodologies alongside automatic packaging techniques in real-world scenarios. Paper C implements Paper A's method to design an innovative rear-axle for electric vehicles, transforming a conventional internal combustion engine suspension to meet electric vehicle packaging requirements while maintaining driving dynamics performance. This optimization employed an automated approach for proposing new hardpoints based on specified requirements, using simplified models to efficiently evaluate packaging feasibility. Paper D combines methodologies from Papers A and B to design a front axle for electric vehicles, presenting an automated approach for kinematics and elastokinematics design with integrated packaging evaluation, significantly reducing solution development time.

Paper E introduces a reinforcement learning (RL) based approach for cascading complete vehicle targets into suspension kinematics targets. This

method achieves superior convergence speed and accuracy compared to traditional multi-objective optimization techniques. The implementation uses a modified Actor-Critic framework inspired by [40], where the RL agent maximizes rewards from a simulation environment. The reward structure is strategically designed to guide suspension kinematics targets toward optimal values, while a probabilistic model effectively captures environmental uncertainties.

This research encompasses broad domains including complete vehicle engineering and suspension engineering, with methods from Papers A, B, and E being applicable to the concept development phase. However, it is important to acknowledge certain methodological limitations and simplifying assumptions.

Paper A primarily addresses suspension targets related to longitudinal and lateral dynamics, while Paper E establishes connections between these suspension targets and complete vehicle performance objectives. Consequently, the research scope is limited to longitudinal and lateral vehicle dynamics targets. The thesis does not address subsystems such as springs, dampers, and tyres that substantially influence vertical dynamics and ride comfort. Furthermore, while Paper B presents a algorithm for suspension compliance, this aspect is not integrated into the approach described in Paper E. The compliance method in Paper B serves as a complementary tool for hardpoint design, ensuring that suspension compliance targets can be achieved through appropriate hardpoint configuration and bushing compliance parameters. Paper D demonstrates a practical application combining methodologies from Papers A and B, though it presents a conceptual asymmetrical design that faces implementation challenges with current technologies. It should also be noted that Paper B focuses exclusively on linear compliance behavior, with bushing preload effects remaining outside the scope of analysis.

#### 1.4 Thesis outline and contribution

This thesis is structured as follows: Chapter 2 is divided into two principal sections—the first elucidates the methodologies established in Papers A and B, while the second examines the innovative approach presented in Paper E. Chapter 3 offers a comprehensive case study demonstrating the practical implementation of these methodologies, beginning with the derivation of suspension targets using the method from Paper E, followed by their cascad-

ing transformation into specific hardpoint configurations and bushing design parameters through the techniques developed in Papers A and B.

#### 1.4.1 Scientific contributions

#### I. Automate the hardpoint design

Traditional suspension design methods based on trial-and-error are not efficient. Suspension engineers must meet packaging constraints by relying on trial-and-error iterative simulations to gradually refine the kinematic performance. Simulating suspension behaviors is also computationally expensive. Therefore, a method that reduces the kinematic design lead time has been proposed. The method presented primarily addresses the kinematic design problem by reversing the traditional design procedure. The algorithm, which starts from target identification, provides design guidelines, including linkage orientation, length, and position. The method includes calculations in two steps. The first step is to obtain the velocity constraints and to use first-order linear targets to calculate general motions. Then the hardpoints design guideline for the first-order targets control is provided from the algorithm to designers by indicating the linkage directions. The second step uses higher-order targets (acceleration and jerk constraints), which can be obtained by partial differentiation from velocity and acceleration constraints. The exact position of the linkage can then be calculated with these higher-order targets. The results show that the general motion, which includes velocity, acceleration, and jerk, is precisely controlled by this method. The result also shows that the complete design can be approached simultaneously from a feasible packaging solution and required kinematic setup, and eventually transfers into a solution that satisfies both packaging and kinematic requirements. The reverse method helps design engineers search for feasible packaging solutions more efficiently in the early design stages. Furthermore, compared with previous optimization-based methods, the new method here always provides unique solutions, which means that the targets and the hardpoints are uniquely correlated. Therefore, engineers who work with CAE and CAD parts can always build clear connections to each other by understanding the influence from both the performance and the packaging side. (Paper A)

#### II. Automate the bushing design

The traditional bushing tuning method involves an optimization process in Adams Car or any other multi-body simulation software. Although it provides reliable results, it is a iterative process to build models for the complete kinematics and compliance analysis. Therefore, a method to reduce the bushing tuning time has been proposed. It applies the reverse algorithms to calculate the bushing stiffness values along the link directly from the compliance targets for a given hardpoint setup and provides guidelines for the proper bushing design in the early phase of the concept development. The method includes the calculation of motion ratios and force distribution as a function of the hardpoint setup. So, regardless of the compliance targets and bushing stiffness values, these ratios remain constant as long as hardpoints are unchanged. Further, these ratios are used to study the possible effect on the wheel orientation if bushings are used as a bushing sensitivity study. Then the exact stiffness of the bushings at the inner hardpoints is calculated by specifying the compliance targets. (Paper B)

## III. An application of automated hardpoint methodology for front axle development

To meet the complex requirements, the design of a new suspension concept is usually labor-intensive. The suspensions' kinematics and packaging need to be considered simultaneously since they influence each other. A method or process for how to design for both kinematic requirements and packaging requirements is developed and demonstrated. The goal of this work is to invent a new suspension system for a battery electric vehicle with a maximized battery volume. The underlying algorithms are used to handle the kinematics and packaging automatically. Critical improvements during the development are demonstrated within showcases and subsequently discussed. The tuning process starts from a suspension used in a traditional combustion vehicle and eventually is adapted to the needs of a battery electric vehicle. The automatic kinematic tuning method is used to maintain the performance targets for each iteration, while the automatic packaging tool is used to search for a feasible packaging solution. The showcases confirm the efficiency of both kinematics and packaging methods. Eventually, the new suspension layout provides an extra 130mm for the battery. The results prove the possibility to synchronize the kinematics tuning and packaging processes. Thanks to the automatic methods, the design lead time has been dramatically reduced. (Paper C)

#### IV. An application of automated hardpoint and bushing design methodology for rear axle development

With rising customer expectations and additional requirements stemming from electrification, today's suspensions need to fulfill an increasing number of requirements: Aerodynamic efficiency targets are stricter, driving properties are defined more specifically, and the use of carryover parts is growing. Moreover, the package volume has a huge effect on the exterior design as well. This leads to complications in the predevelopment process. A typical problem is the sequence of development steps: if a completely new suspension is designed, is it more important to optimize the hard points and adjust the part geometry accordingly or vice versa? The common approach of a trial-and-error method is time-consuming since the design of a suspension concept takes days of engineering work. To meet this dilemma, a new approach is developed. With an automated design method for kinematics and elastokinematics paired with an automatic packaging evaluation, it is possible to create a first feasible solution within minutes. This concept can then be evaluated and improved either in terms of hard points, bushing stiffness, or packaging. Since a much higher amount of possible suspension designs can be evaluated, the probability of finding an adequate solution rises tremendously. This approach is demonstrated for an optimized fivelink suspension for battery-electric vehicles (BEVs). The shape of the suspension volume should be modified in a way that the height of the engine hood can be lowered. Therefore, the aerodynamic behavior has the potential to be improved. It is found that the design of an innovative concept solution can be supported by using automated methods. (Paper D)

#### V. A method to set up suspension targets

Setting up suspension kinematics targets has been a challenging task for vehicle engineers. The challenges involve a high-dimensional search space, non-linear relationships between the suspension kinematics and vehicle dynamics, exploration and exploitation trade-offs, and the need for domain-specific knowledge. The traditional approach is to use multiobjective optimization, which is computationally expensive and rarely converges to the global optimal solution in high-dimensional cases. In this paper, we investigate a new method to find optimal suspension kinematics targets using reinforcement learning. The method is based on the accumulation of knowledge through the interaction between an intelligent agent and a simulation environment. The agent optimizes suspension kinematics targets by receiving rewards tied to vehicle dynamics performance. The results show that the proposed method can find optimal suspension kinematics targets with the help of accumulated knowledge. The knowledge-guided learning process can replace traditional optimization with less convergence time and better results. The proposed method has the potential to revolutionize the way suspension kinematics targets are set up in the automotive industry. (Paper E)

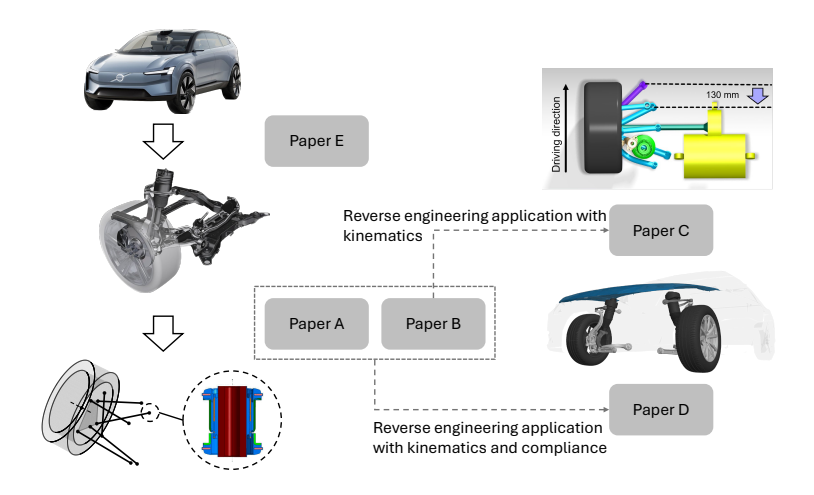


Figure 1.2. Interconnections among the appended papers

Figure 1.2 illustrates the interconnections among the appended papers. Paper E establishes a framework for determining suspension kinematics targets, which Paper A subsequently utilizes to configure suspension hardpoints. The practical application of Paper A's algorithm is demonstrated through a rear

suspension case study. Similarly, the suspension compliance methodology from Paper B, which enables systematic bushing stiffness configuration, is validated through application examples. Paper D synthesizes methodologies from both Papers A and B, presenting a comprehensive front suspension design demonstration.

Before proceeding to subsequent chapters, it is important to emphasize that this thesis directly addresses the challenges identified in Section 1.2. The presented concepts, theories, and methodologies collectively aim to enhance the efficiency of suspension design during the critical concept phase.

#### 1.4.2 Organizational and societal contributions

The specific contributions to both organizational effectiveness and broader societal impact are enumerated below.

- I. Enhance organizational capability to develop innovative vehicle concepts where suspension systems serve as integral components.
- II. Strengthen competitive advantage in chassis design while reducing development lead-time—particularly crucial during the industry's transition toward electric propulsion and autonomous driving technologies.
- III. Advance knowledge in AI-supported, data-driven product development and vehicle dimensioning, optimizing the interaction between engineering expertise and artificial intelligence methodologies.
- IV. Provide frameworks for improved system understanding and efficient large-scale optimization in product and architectural development processes.
- V. Refine modeling approaches, virtual methodologies, and requirement specifications for complex suspension design phenomena.
- VI. Strengthen decision support and risk assessment in vehicle development by establishing clear relationships between product requirements and design parameters during the concept phase.

#### CHAPTER 2

Method

This chapter discusses the methods that address the research question in Section 1.2. Starting with the kinematics and compliance reverse engineering method, followed by the reinforcement learning method. A common interface is set for both methods. Therefore, a development method from complete vehicle behavior to hardpoint and bushing setup is possible.

#### 2.1 Kinematics and compliance

#### 2.1.1 Model

#### 2.1.1.1 Modelling of the multilink axle

The modelling part consists of velocity, acceleration and jerk analyses. Jerk as the time derivative of acceleration is studied by I. and M. [41]. The velocity and angular velocity at wheel center are calculated using velocity constraints. Then Jacobian methods are used to derive the acceleration as well as the jerk motions.

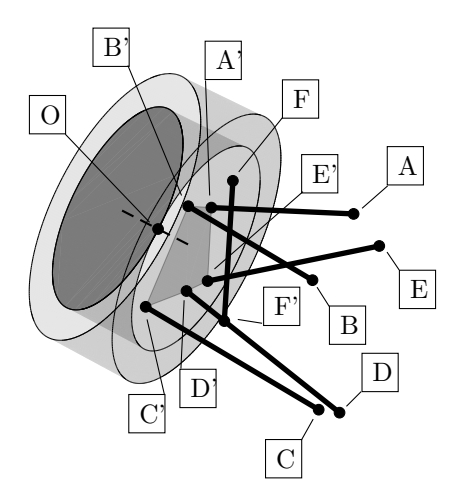


Figure 2.1. Mulitilink rear suspension and nomenclature

**Velocity constraints** The velocity analysis solves the general motion  $V_o, \omega_o$  at wheel center for jounce and steer motions. A simple model to calculate jounce motion for multilink is demonstrated. Equation 2.1 shows the velocity constraint for each individual link with the reference from Figure 2.1.

$$(\mathbf{V}_o + \omega_o \times \mathbf{L}_{i'o}) \cdot \mathbf{L}_{i'i} = 0 \tag{2.1}$$

where,

$$i = A, B, C, D, E$$
  
 $\mathbf{L}_{i'i} = d(i, i'), d$  is the euclidean distance  $\mathbf{L}_{i'o} = d(i', o)$ 

Equation 2.1 can be written with matrix form with generalized coordinates  $\dot{q} = [\mathbf{V}_o^T, \omega_o^T]^T$  and Jacobian matrix  $[C_q]$ . Equation 2.2 can be partitioned as

Equation 2.3.

$$[C_q] \cdot \dot{\mathbf{q}} = 0 \tag{2.2}$$

$$[C_u] \cdot \dot{\mathbf{u}} - [C_w] \cdot \dot{\mathbf{w}} = 0 \tag{2.3}$$

where,

$$\dot{\mathbf{u}} = [V_{ox}, V_{oy}, \omega_{ox}, \omega_{oy}, \omega_{oz}] 
\dot{\mathbf{w}} = V_{oz} 
[C_u] \text{ shown in Paper A} 
[C_w] \text{ shown in Paper A}$$

With  $V_{oz}$  given,  $\dot{\mathbf{u}}$  can be calculated and the general velocities at wheel center point O are then known. The velocities of any hardpoints at knuckle can be calculated as Equation 2.4

$$\mathbf{V}_i' = \mathbf{V}_o + \omega_o \times \mathbf{L}_{i'o} \tag{2.4}$$

where,

$$i = A, B, C, D, E$$

Steering motion velocity constraints follow the same derivation as Equation 2.1.  $\mathbf{L}_{F'F}$  should keep length fixed while applying steering motion from toelink  $\mathbf{L}_{C'C}$ . However, the mechanism of  $\mathbf{L}_{D'D}$ ,  $\mathbf{L}_{F'F}$  needs to be modelled with additional generalized coordinates. The steering feature will not be further included in the example of the present paper.

**Acceleration constraints** The acceleration constraints Equation 2.5 can be derived from differentiation of the Equation 2.2.

$$[C_q]\ddot{\mathbf{q}} + [\dot{C}_q]\dot{\mathbf{q}} = 0 \tag{2.5}$$

where,

$$[\dot{C}_q]$$
 shown in Paper A

Similarly, Equation 2.5 can be partitioned as Equation 2.6.

$$[C_u]\ddot{\mathbf{u}} - [C_w]\ddot{\mathbf{w}} + [\dot{C}_a]\dot{\mathbf{q}} = 0 \tag{2.6}$$

where,

$$\mathbf{\ddot{u}} = [a_{ox}, a_{oy}, \alpha_{ox}, \alpha_{oy}, \alpha_{oz}]$$

Paper A shows that  $\dot{C}_q$  is proportional to  $\dot{\mathbf{q}}$ . As a result, Equation 2.6 shows a linear relationship between  $\ddot{\mathbf{u}}$  and  $\dot{\mathbf{q}}^2$  if and only if  $\ddot{\mathbf{w}}$  is zero. So,  $\ddot{\mathbf{w}}$  is zero because  $V_{Oz}$  is given as constant. Furthermore, this assumption will simplify the derivation of the jerk motions.  $\ddot{\mathbf{u}}$  can be calculated from given  $\dot{\mathbf{q}}$  as Equation 2.7. Then the acceleration of any hardpoints at knuckle can be calculated as Equation 2.8.

$$[C_u]\ddot{\mathbf{u}} + [\dot{C}_q]\dot{\mathbf{q}} = 0 \tag{2.7}$$

$$\mathbf{a}_{i}' = \mathbf{a}_{o} + \alpha_{o} \times \mathbf{L}_{i'o} + \omega_{o} \times (\omega_{o} \times \mathbf{L}_{i'o}) \tag{2.8}$$

where,

$$i = A, B, C, D, E$$

**Jerk constraints** The jerk motion  $\ddot{\mathbf{u}}$  is the time derivative of acceleration. Considering derivative of Equation 2.7 with respect to time, Equation 2.9 can be formulated. Since  $\ddot{\mathbf{w}}$  is assumed to be zero,  $[\dot{C}_q]\ddot{\mathbf{q}}$  is equal to  $[\dot{C}_u]\ddot{\mathbf{u}}$ . Therefore, Equation 2.9 can be rewritten as Equation 2.10.

$$[\dot{C}_u]\ddot{\mathbf{u}} + [C_u]\ddot{\mathbf{u}} + [\ddot{C}_q]\dot{\mathbf{q}} + [\dot{C}_q]\ddot{\mathbf{q}} = 0$$
(2.9)

$$2 \cdot [\dot{C}_q]\ddot{\mathbf{q}} + [C_u]\ddot{\mathbf{u}} + [\ddot{C}_q]\dot{\mathbf{q}} = 0$$
 (2.10)

where,

$$\begin{split} & [\ddot{C}_q] \text{ shown in Paper A} \\ & \dddot{\mathbf{u}} = [j_{ox}, j_{oy}, \phi_{ox}, \phi_{oy}, \phi_{oz}] \end{split}$$

As a summary,  $\dot{\mathbf{u}}$ ,  $\ddot{\mathbf{u}}$ ,  $\ddot{\mathbf{u}}$  can be calculated with hardpoints and  $\dot{\mathbf{w}}$  which is  $V_{Oz}$  for the jounce motion. The general motions  $\dot{\mathbf{q}}$ ,  $\ddot{\mathbf{q}}$ ,  $\ddot{\mathbf{q}}$  will be used to define targets.

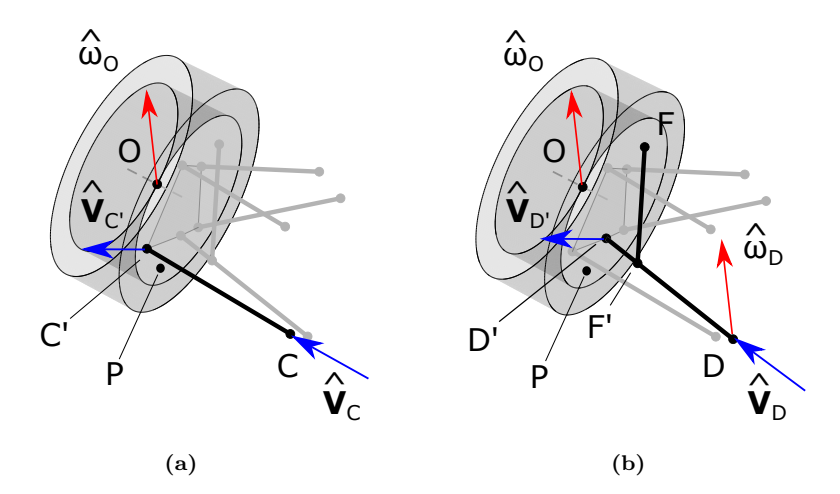


Figure 2.2. Motion ratio calculation for support links(a) and spring link(b)

#### 2.1.1.2 Motion ratio calculation

To capture the motion of wheel center O from the movement of the individual bushing. The motion ratios need to be calculated according to kinematic constraints. A method-based linearized constraint was introduced by Matschinsky [23]. This section will modify the method and obtain the motion ratios between the wheel center and bushing radial directions.

To model the kinematic constraints, two types of constraints are shown in Figure 2.2. They are distinguished by the spring link and support link. The motion at wheel  $\hat{\mathbf{V}}_O$  and  $\hat{\omega}_O$  are interesting with the given velocity at hardpoint A, B, C, D, and E. Equation 2.11 shows the motion depending on the hardpoint and input velocity at each inner hardpoint. Assume a constant velocity v is applied on each inner hardpoint, therefore the motions at wheel center O are proportional to v for each specific hardpoint configuration.

$$[\hat{\mathbf{V}}_O^i, \hat{\omega}_O^i] = f_i(\mathrm{HP}, \hat{\mathbf{V}}_i) \tag{2.11}$$

where,

$$i = A, B, C, D, E$$

To calculate the motion at the wheel center O, the velocity constraints for the spring link and the support links need to be constructed. To simplify the expression, the unknown parameters are  $\hat{\mathbf{V}}_{D'}$ ,  $\hat{\omega}_{O}$ , and  $\hat{\omega}_{D}$ .

For the spring link (D - D') in Figure 2.2b,

$$\hat{\mathbf{V}}_{D'} + \hat{\omega}_D \times \mathbf{L}_{D'D} = \hat{\mathbf{V}}_D = v \cdot \hat{\mathbf{e}}_{D'D}$$
 (2.12)

$$(\hat{\mathbf{V}}_{D'} + \hat{\omega}_D \times \mathbf{L}_{F'D}) \cdot \hat{\mathbf{e}}_{F'F} = 0 \tag{2.13}$$

where,

 $\mathbf{L}_{D'D} = d(D'D), \ d$  is the euclidean distance  $\mathbf{L}_{F'D} = d(F'D), \ d$  is the euclidean distance  $\hat{\mathbf{e}}_{D'D}$  is unit vector of  $\mathbf{L}_{D'D}$   $\hat{\mathbf{e}}_{F'F}$  is unit vector of  $\mathbf{L}_{F'F}$ 

For the toe link (C - C') in Figure 2.2a,

$$(\hat{\mathbf{V}}_{D'} + \hat{\omega}_O \times \mathbf{L}_{D'i'}) \cdot \mathbf{L}_{i'i} = \mathbf{L}_{i'i} \cdot \hat{\mathbf{V}}_i$$
(2.14)

where,

$$\mathbf{L}_{i'i} = d(i'i), \ d$$
 is the euclidean distance  $i = A, B, C, E$ 

In addition to the constraints from Equation 2.12 to Equation 2.14. The rotation of link  $\mathbf{L}_{D'D}$  need to be specified, for example,  $\hat{\omega}_D \cdot \mathbf{L}_{D'D} = 0$ . The equations can be written in a matrix format with unknown parameters  $\hat{\omega}_O$ ,  $\hat{\omega}_D$ , and  $\hat{\mathbf{v}}_{D'}$ . The velocity at hardpoint D' and rotational velocity can be calculated using linear algebra. The velocity at wheel center O can be calculated as the Equation 2.15,

$$\hat{\mathbf{V}}_O = \hat{\mathbf{V}}_{D'} + \hat{\omega}_O \times \mathbf{L}_{OD'} \tag{2.15}$$

For given hardpoints, the motion ratios can be obtained by given input velocity at each inner hardpoionts.

$$[\hat{\mathbf{V}}_{O}^{i}, \hat{\omega}_{O}^{i}] = f(|\hat{\mathbf{V}}_{i}| = v, |\hat{\mathbf{V}}_{else}| = 0)$$
 (2.16)

where,

$$i = A, B, C, D, E$$

$$[\hat{\mathbf{V}}_O^i, \hat{\omega}_O^i] = f_i(v) \tag{2.17}$$

where,

$$i = A, B, C, D, E$$

#### 2.1.1.3 Force distribution

From Equations 2.12, 2.13 and 2.15, it is possible to form a linear matrix to solve the kinematic constraint equations to capture the motion at wheel center O. The input velocities from A, B, C, D and E can be expressed as the bushing deformations along the link directions for a particular load case. The bushing deformations are calculated using Hooke's law  $F = -K \cdot x$  equation. where K is the bushing stiffness and if a force F acts on the bushing, it deforms by the amount x in the direction of the equilibrium position. Therefore, it becomes necessary to calculate the forces acting on each bush.

The wheel suspension system can be divided into individual parts to calculate the force distribution using free-body diagrams.  $F_{Px}$ ,  $F_{Py}$ ,  $F_{Pz}$  and  $M_{Px}$ ,  $M_{Py}$ ,  $M_{Pz}$  be the input forces and moments at the tyre contact point P in the tyre coordinate system. As this paper does not focus on the tyre, the suspension knuckle and tyre can be considered as a single rigid body. The force equilibrium equations for the knuckle:

$$F_O + F_{A'} \cdot \hat{e}_{A'A} + F_{B'} \cdot \hat{e}_{B'B} + F_{C'} \cdot \hat{e}_{C'C} + F_{D'} \cdot \hat{e}_{D'D} + F_{E'} \cdot \hat{e}_{E'E} = 0 \quad (2.18)$$
 where,

$$F_O = \begin{bmatrix} F_{Px} \cdot \cos(\delta) + F_{Py} \cdot \sin(\delta) \\ F_{Py} \cdot \cos(\delta) - F_{Px} \cdot \sin(\delta) \\ F_{Pz} \end{bmatrix}$$

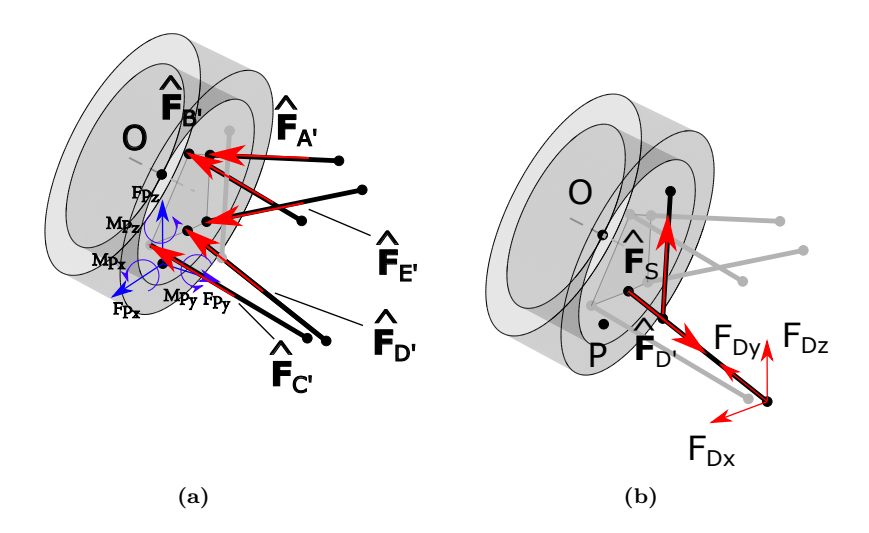


**Figure 2.3.** Force ratio calculation for support links(a) and spring link(b)

Taking moment equilibrium about point D':

$$(M_O + (L_{OD'} \times F_O)) + F_{A'} \cdot (L_{A'D'} \times \hat{e}_{A'A}) + F_{B'} \cdot (L_{B'D'} \times \hat{e}_{B'B}) + F_{C'} \cdot (L_{C'D'} \times \hat{e}_{C'C}) + F_{E'} \cdot (L_{E'D'} \times \hat{e}_{E'E}) = 0$$
(2.19)

where,

$$M_O = \begin{bmatrix} M_{Px} \\ M_{Py} \\ M_{Pz} \end{bmatrix} + (L_{P,O} \times F_O)$$

Notice  $F_O$  and  $M_O$  are the forces and moments at the wheel center in the global coordinate system.

Force equilibrium equations for links can be:

$$-F_{i'} \cdot \hat{e}_{i'i} + K_i \cdot S_i \cdot \hat{e}_{i'i} = 0$$
 (2.20)

$$K_i$$
 = Bushing radial stiffness at D  
 $S_i$  = Bushing deformation at D  
 $i$  = A.B.C.E

Considering the forces acting along the link direction i'i the moment equations are eliminated. However, for the spring link, the moments need to be included due to the force  $F_s$  from the spring itself.

Force equilibrium equations for spring link:

$$-F_{D'} \cdot \hat{e}_{D'D} + K_S \cdot S \cdot \hat{e}_{F'F} + K_D \cdot S_D \cdot \hat{e}_{D'D} = 0 \tag{2.21}$$

Taking moment equilibrium about Point D:

$$-F_{D'} \cdot (L_{DD'} \times \hat{e}_{D'D}) + K_S \cdot (L_{DF'} \times \hat{e}_{F'F}) = 0$$
 (2.22)

From all these equations, a linear force matrix from Paper B equation can be formed to calculate the force distribution at different joints and bushings for a particular input load case. And the ratios  $\frac{F_i}{F_{Px}}$ ,  $\frac{F_i}{F_{Py}}$ ,  $\frac{F_i}{F_{Pz}}$  for different bushings are calculated.

In general, for a given hardpoint setup, the forces in the bushings can be represented as a function of the input force at the tyre contact point or the wheel center.

$$[F_i] = g_i(F_j) \tag{2.23}$$

where,

i = A, B, C, D, E

j = Px, Py, Pz, Ox, Oy, Oz (Input forces at contact point P or wheel center O)

## 2.1.2 Target identification

This section describes the targets and their definitions used for the kinematics and compliance reverse engineering method.

#### 2.1.2.1 Kinematics target

The first order targets are defined using velocities and angular velocities. They represent the change of position measurements at wheel center and contact

point. The contact point between the tyre and ground is named P, and toe  $\delta$  and camber  $\gamma$  define the wheel orientation. For steering motion, the velocities and angular velocities measured at point O are  $\mathbf{V}_o', \omega_o'$ . The velocity at contact point can be calculated as Equation 2.24 and 2.25. Equation 2.26-2.35 define the targets in detail sense. The definitions are recalled from Y. [42] at reference coordinate system.

$$\mathbf{V}_P = \mathbf{V}_o + \omega_o \times \mathbf{L}_{po} \tag{2.24}$$

$$\mathbf{V}_{P}^{'} = \mathbf{V}_{o}^{'} + \omega_{o}^{'} \times \mathbf{L}_{po} \tag{2.25}$$

$$1^{st} \text{ Bump Steer} = \frac{\omega_{\delta}}{V_{oz}}$$
 (2.26)

$$1^{st} \text{ Bump Camber} = \frac{\omega_{ox} \cos(\delta) - \omega_{oy} \sin(\delta)}{V_{oz}}$$
 (2.27)

(Kinematic) 
$$1^{st}$$
 Anti-squat =  $\frac{V_{ox}}{V_{oz}}$  (2.28)

(Kinematic) 
$$1^{st}$$
 Anti-lift =  $\frac{V_{Px}}{V_{Pz}}$  (2.29)

$$1^{st} \text{ RCH} = P_y \cdot \frac{V_{Py}}{V_{Pz}} \tag{2.30}$$

$$\text{Hub Trail} = \frac{-(V_{oy}^{'}\cos(\delta) + V_{ox}^{'}\sin(\delta))}{\omega_{\delta}^{'}} \tag{2.31}$$

Kingpin offset = 
$$\frac{V_{ox}^{'}\cos(\delta) - V_{oy}^{'}\sin(\delta)}{\omega_{\delta}^{'}}$$
 (2.32)

Caster trail = 
$$\frac{-(V_{px}^{'}\sin(\delta) + V_{py}^{'}\cos(\delta))}{\omega_{\delta}^{'}}$$
 (2.33)

Scrub radius = 
$$\frac{V_{px}^{'}\cos(\delta) - V_{py}^{'}\sin(\delta)}{\omega_{\delta}^{'}}$$
 (2.34)

Wheel load level arm (WLLA) = 
$$\frac{V_{pz}^{'}}{\omega_{\delta}^{'}}$$
 (2.35)

$$\omega_{\delta} = -\omega_{x} \tan(\gamma) \sin(\delta) - \omega_{y} \tan(\gamma) \cos(\delta) + \omega_{z}$$
  
$$\omega_{\delta}^{'} = -\omega_{ox}^{'} \tan(\gamma) \sin(\delta) - \omega_{oy}^{'} \tan(\gamma) \cos(\delta) + \omega_{oz}^{'}$$

The second order targets are defined as the time derivative of the first order targets with respect to time. They represent the changes of the velocities. Notice that the second order targets are always defined as targets versus  $V_z$  to make them independent of input velocity. The derivations assume a constant toe, camber angle and the fixed contact position to simplify the expressions. The acceleration at contact point can be calculated as Equation 2.36.

$$\mathbf{a}_p = \mathbf{a}_o + \alpha_o \times \mathbf{L}_{op} + \omega_o \times (\omega_o \times \mathbf{L}_{op}) \tag{2.36}$$

$$2^{nd} \text{Bump Steer} = \frac{\frac{d}{dt} \text{Bump Steer}}{V_{oz}} = \frac{\alpha_{\delta}}{V_{oz}^2}$$
 (2.37)

$$2^{nd} \text{Bump camber} = \frac{\frac{d}{dt} \text{Bump camber}}{V_{oz}} = \frac{\alpha_{ox} \cos(\delta) - \alpha_{oy} \sin(\delta)}{V_{oz}^2} \qquad (2.38)$$

$$2^{nd} \text{Anti squat} = \frac{\frac{d}{dt} \text{Anti squat}}{V_{oz}} = \frac{a_{ox} V_{oz} - a_{oz} V_{ox}}{V_{oz}^3}$$
(2.39)

$$2^{nd} \text{Anti lift} = \frac{\frac{d}{dt} \text{Anti lift}}{V_{oz}} = \frac{a_{px} V_{pz} - a_{pz} V_{px}}{V_{nz}^2 V_{oz}}$$
(2.40)

$$2^{nd} \text{RCH} = \frac{\frac{d}{dt} \text{RCH}}{V_{oz}} = P_y \cdot \frac{a_{py} V_{pz} - a_{pz} V_{py}}{V_{pz}^2 V_{oz}}$$
(2.41)

where,

$$\alpha_{\delta} = -\alpha_{ox} \tan(\gamma) \sin(\delta) - \alpha_{oy} \tan(\gamma) \cos(\delta) + \alpha_{oz}$$

For a steerable front axle, additional targets are identified here. To define the measure of the target, the general motion at wheel center assume to be known. The method to derive the general motion is described in Paper A. The general motion  $\mathbf{V}'$ ,  $\mathbf{a}'$ ,  $\mathbf{a}'$  at wheel center and  $\mathbf{V}'_p$ ,  $\mathbf{a}'_p$  at contact point can be calculated using same method.

$$2^{\rm nd} \text{ kingpin angle} = \frac{1}{1 + \frac{\omega_x'^2}{\omega_z'^2}} \cdot \frac{\alpha_x'}{\omega_z'^2}$$
 (2.42)

$$\begin{split} 2^{\text{nd}} \text{ Scrub Radius} &= \frac{(a_{px}^{'}\cos(\delta) - a_{py}^{'}\sin(\delta))\omega_{\delta}^{'}}{\omega_{\delta}^{'2}\omega_{z}^{'}} \\ &- \frac{\alpha_{\delta}^{'}(V_{px}^{'}\cos(\delta) - V_{py}^{'}\sin(\delta))}{\omega_{\delta}^{'2}\omega_{z}^{'}} \end{split} \tag{2.43}$$

$$2^{\rm nd} \text{ caster angle} = \frac{1}{1 + \frac{\omega_y'^2}{\omega_z'^2}} \cdot \frac{\alpha_y'}{\omega_z'^2}$$
 (2.44)

$$\begin{split} 2^{\text{nd}} \text{ Caster trail} &= \frac{(-a_{px}^{'}\sin(\delta) - a_{py}^{'}\cos(\delta))\omega_{\delta}^{'}}{\omega_{\delta}^{'2}\omega_{z}^{'}} \\ &- \frac{\alpha_{\delta}^{'}(-V_{px}^{'}\sin(\delta) - V_{py}^{'}\cos(\delta))}{\omega_{\delta}^{'2}\omega_{z}^{'}} \end{split} \tag{2.45}$$

$$2^{\text{nd}} \text{ WLLA} = \frac{a'_{pz}\omega'_{\delta} - \alpha'_{\delta}V'_{z}}{\omega'_{\delta}^{2}\omega'_{z}}$$
 (2.46)

$$\begin{split} \omega_{\delta}^{'} &= -\omega_{x}^{'}\tan(\gamma)\sin(\delta) - \omega_{y}^{'}\tan(\gamma)\cos(\delta) + \omega_{z}^{'}\\ \alpha_{\delta}^{'} &= -\alpha_{x}^{'}\tan(\gamma)\sin(\delta) - \alpha_{y}^{'}\tan(\gamma)\cos(\delta) + \alpha_{z}^{'} \end{split}$$

Similar to the second order targets, the third order targets are defined as the time derivative of the second order targets respect to time. Notice that the third order targets always are defined as targets versus  $V_z^2$  to making them independent of input velocity. The translational jerk at contact point can be calculated as Equation 2.47.

$$\mathbf{j}_{p} = \mathbf{j}_{o} + \phi_{o} \times \mathbf{L}_{op} + 2\alpha_{o} \times (\omega_{o} \times \mathbf{L}_{op}) + \omega_{o} \times (\alpha_{o} \times \mathbf{L}_{op}) + \omega_{o} \times (\omega_{o} \times (\omega_{o} \times \mathbf{L}_{op}))$$

$$(2.47)$$

$$3^{rd}$$
Bump Steer =  $\frac{\frac{d^2}{dt^2}$ Bump Steer  $\frac{j_{\delta}}{V_{oz}^2} = \frac{j_{\delta}}{V_{oz}^3}$  (2.48)

$$3^{rd} \text{Bump Camber} = \frac{\frac{d^2}{dt^2} \text{Bump Camber}}{V_{oz}^2} = \frac{j_{ox} \cos(\delta) - j_{oy} \sin(\delta)}{V_{oz}^3}$$
(2.49)

$$3^{rd}$$
Anti Squat =  $\frac{\frac{d^2}{dt^2}$ Anti Squat  $V_{ox}^2 = \frac{j_{ox}}{V_x^3}$  (2.50)

$$3^{rd} \text{Anti Lift} = \frac{\frac{d^2}{dt^2} \text{Anti Lift}}{V_{oz}^2} = \frac{j_{px} V_{oz} - j_{pz} V_{ox} - a_{pz} a_{ox}}{V_{pz}^2 V_{oz}^2} - \frac{2a_{pz} (a_{px} V_{oz} - a_{pz} V_{ox})}{V_{0z}^3 V_{oz}^2}$$
(2.51)

$$3^{rd}RCH = \frac{\frac{d^2}{dt^2}RCH}{V_{oz}^2} = \frac{P_y}{V_{oz}^2} \cdot \left[ \frac{j_{py}V_{pz} + a_{py}a_{pz} - j_{pz}V_{py} - a_{pz}a_{py}}{V_{pz}^2} - \frac{2a_{pz}(a_{py}V_{pz} - a_{pz}V_{py})}{V_{oz}^3} \right]$$
(2.52)

$$j_{\delta} = -j_{ox} \tan(\gamma) \sin(\delta) - j_{oy} \tan(\gamma) \cos(\delta) + j_{oz}$$

In summary, the general motions  $\dot{\mathbf{q}}, \ddot{\mathbf{q}}, \ddot{\mathbf{q}}$  which were calculated from Section 2.1.1.1 are transferred to the targets, and engineers use the targets to evaluate the kinematic performance.

#### 2.1.2.2 Compliance target

The wheel motions under certain force which applied on the tyre contact patch are described using compliance targets. The targets describe the motion mainly under braking force and lateral force. Table 2.1 shows the selected targets. The combined compliance effects from all the bushings need to meet the targets in order to provide safe and stable driving behaviors. The targets monitor the toe  $\delta$ , camber  $\gamma$ , and other motions of wheel center O and contact point P. The definitions are shown in the Equations 2.53-2.57.

Table 2.1. Compliance targets

*	
Brake steer	
Longitudinal compliance	e
Wind-up stiffness	
lateral force steer	
lateral force camber	

Brake steer = 
$$\frac{\delta}{F_{px}}$$
 (2.53)

Longitudinal compliance = 
$$\frac{O_x}{F_{Ox}}$$
 (2.54)

Wind-up stiffness = 
$$\frac{\angle Oy}{F_{px}}$$
 (2.55)

Lateral force steer = 
$$\frac{\delta}{F_{py}}$$
 (2.56)

$$\text{Lateral force camber} = \frac{\gamma}{F_{py}} \tag{2.57}$$

The targets identified above are the motion gradients from the combined bushing effects. Therefore, the targets should be identified as time derivatives from Equations 2.53-2.57. To simplify the expression, static toe and camber angle assume to be zero. Then the targets are modified as following expressions.

$$\frac{d}{dt} \text{Brake steer} = \frac{\omega_z}{F_{px}} \tag{2.58}$$

$$\frac{d}{dt}\text{Longitudinal compliance} = \frac{V_{Ox}}{F_{Ox}}$$
 (2.59)

$$\frac{d}{dt} \text{Wind-up stiffness} = \frac{\omega_y}{F_{px}}$$
 (2.60)

$$\frac{d}{dt}\text{Lateral force steer} = \frac{\omega_z}{F_{py}} \tag{2.61}$$

$$\frac{d}{dt} \text{Lateral force camber} = \frac{\omega_x}{F_{py}}$$
 (2.62)

#### 2.1.3 Target-driven reverse design method

The method is to reverse the traditional design process. The reverse algorithm collects the performance targets as input. Then the targets are transferred to general motions and hardpoints are proposed according to general motions. The reverse method introduces control point concept and geometrical guidelines. Figure 2.4 describes the method step by step.

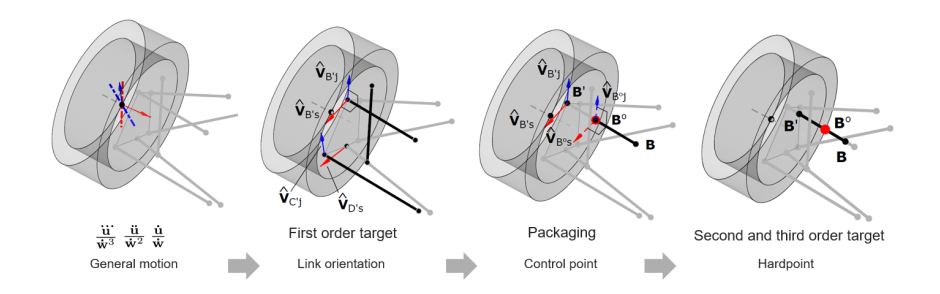


Figure 2.4. Kinematics reverse design process

**General motions** The general motions, which include jounce motion up to third order and steering motion with first order, can be calculated from targets which are shown in Section 2.1.2 with a symbolic solver. The relations are already derived in Section 2.1.1.

**Links orientation** The design purpose is to find a setup which gives the general motions while applying jounce and steering motions. The reverse design starts with hardpoints at knuckle. Since the knuckle is a rigid body, the velocities  $\hat{\mathbf{V}}_{i'j}$ ,  $\hat{\mathbf{V}}_{i's}$  of any hardpoints at the knuckle can be calculated as Equation 2.63.

$$\hat{\mathbf{V}}_{i'} = \hat{\mathbf{V}}_o + \hat{\omega} \times \mathbf{L}_{i'o} \tag{2.63}$$

where,

$$i = A, B, C, D, E$$

The links  $\mathbf{L}_{A'A}$ ,  $\mathbf{L}_{B'B}$ ,  $\mathbf{L}_{D'D}$ ,  $\mathbf{L}_{E'E}$  which control steering and jounce motions, are called support links. The link  $\mathbf{L}_{C'C}$  which controls steering motion, is called toelink, and link  $\mathbf{L}_{F'F}$ , which controls jounce motion is called spring link. Figure 2.4 indicates the critical vectors to support links design. The support link, for example B'B, should be orthogonal to  $\hat{\mathbf{V}}_{B's}$  and  $\hat{\mathbf{V}}_{B'j}$ . Therefore, the orientations for the support links are defined with the given point i'.

The toe link should be perpendicular to  $\hat{\mathbf{V}}_{C'j}$  and the spring link should be perpendicular to  $\hat{\mathbf{V}}_{C'j}$ . However, their orientations are not uniquely defined. In order to uniquely determine the orientations of the toe link and spring link, additional hardpoints should be given as input. For example, hardpoints components  $C_{dirx}$ ,  $C_{diry}$  and  $F'_y$ ,  $F_y$ ,  $F_z$  can be used to specify the direction of the toe link and the spring link. The hardpoint  $F'_y$  has great influence on the spring ratio, therefore, the position of this point should consider the kinematic performance and the packaging constraints simultaneously.

The control points As Section 2.1.3 described, the orientation of the support link  $L_{B'B}$  is controlled by the hardpoint B' and the first order general motions. A new auxiliary point  $B^o$  located on the support link  $L_{B'B}$  is introduced from Figure 2.4. The velocity vectors  $\hat{\mathbf{V}}_{B^o j}$  and  $\hat{\mathbf{V}}_{B^o s}$  are rotating with respect to the support link  $L_{B'B}$  from the velocity vectors  $\hat{\mathbf{V}}_{B'j}$  and  $\hat{\mathbf{V}}_{B's}$  because of the proportional term  $\hat{\omega} \times \mathbf{L}_{i'o}$  from Equation 2.63. Therefore, the velocity vectors of any hardpoints along the support link  $L_{B'B}$  are orthogonal to the support link  $L_{B'B}$ . In other words, the orientation of the support link  $L_{B'B}$  are controlled by the auxiliary hardpoint  $B^o$  and first order general motions, and the hardpoints B' and B can be any points located on the link which controlled by the auxiliary hardpoint  $B^o$  and first order general motions. Thus the auxiliary hardpoint  $B^o$  is named as the control point for link  $L_{B'B}$ .

In summary, the combinations of the control points and the links orientations can control the first order targets. The hardpoints tuning possibilities have been reduced by means of pre-defined performance targets. The method is also called the linear control method because the method only controls the kinematic behaviors at design position. In order to precisely control the complete kinematic behaviors, the nonlinear kinematic control method is introduced in the next section.

A polynomial approach A toe curve approach with a polynomial of wheel center height (WCH) as a single indeterminate is expressed in Equation 2.64. Figure 2.5 shows three configurations with the same first order coefficients. The blue curve has a smaller second order coefficient compared to the black curve, and the red curve has a larger third order coefficient than the black curve. Figure 2.5 also indicates that the second order coefficient adds a 'C-shaped' curve and third order coefficient adds a 'S-shaped' curve. Therefore, the nonlinear behaviors of the toe curve can be modified by second and third order coefficients. The general motions of second order  $\ddot{\mathbf{q}}$  and third order  $\ddot{\mathbf{q}}$  introduced in Section 2.1.1.1 have similar effects, but they are applied on high dimension cases. A method using second order and third order motions to control hardpoints will be introduced in next section.

$$Toe = a \cdot WCH + b \cdot WCH^2 + c \cdot WCH^3 \tag{2.64}$$

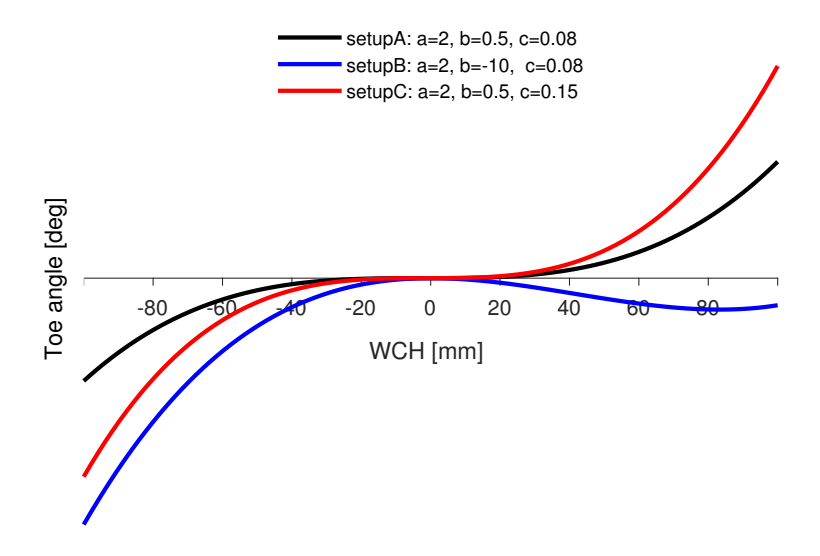


Figure 2.5. The polynomial nonlinear kinematic control approach

**Link length and position** Section 2.1.1.1 shows the method to calculate  $\dot{\mathbf{u}}$ ,  $\ddot{\mathbf{u}}$ ,  $\ddot{\mathbf{u}}$  with given  $\dot{\mathbf{w}}$ . Equations 2.65 show the general motions  $\ddot{\mathbf{u}}$  depend on only the hardpoints layout with input velocity  $\dot{\mathbf{w}}$ . By using the similar derivations, it can be proven that general motions  $\dot{\mathbf{u}}$ ,  $\ddot{\mathbf{u}}$  depend on only the hardpoints layout with input velocity  $\dot{\mathbf{w}}$  as well.

$$\ddot{\mathbf{u}} = \frac{1}{|C_{u}|} \left[ -2[\dot{C}_{u}]\ddot{\mathbf{u}} - [\ddot{C}_{q}]\dot{\mathbf{q}} \right] 
= \frac{1}{|C_{u}|} \left[ -2[\dot{C}_{u}] \frac{-[\dot{C}_{q}]\dot{\mathbf{q}}}{|C_{u}|} - [\ddot{C}_{q}]\dot{\mathbf{q}} \right] 
= \frac{1}{|C_{u}|} \left[ -2[K_{1}]\dot{\mathbf{q}} \frac{-[K_{2}]\dot{\mathbf{q}}\dot{\mathbf{q}}}{|C_{u}|} - [K_{3}]\ddot{\mathbf{q}}\dot{\mathbf{q}} \right] 
= \frac{1}{|C_{u}|} \left[ -2[K_{1}]\dot{\mathbf{q}} \frac{-[K_{2}]\dot{\mathbf{q}}\dot{\mathbf{q}}}{|C_{u}|} - [K_{3}] \frac{-[\dot{C}_{q}]}{|C_{q}|}\dot{\mathbf{q}}\dot{\mathbf{q}} \right] 
= \frac{1}{|C_{u}|} \left[ -2[K_{1}]\dot{\mathbf{q}} \frac{-[K_{2}]\dot{\mathbf{q}}\dot{\mathbf{q}}}{|C_{u}|} - [K_{3}] \frac{-[K_{2}]\dot{\mathbf{q}}}{|C_{q}|}\dot{\mathbf{q}}\dot{\mathbf{q}} \right] 
= \frac{1}{|C_{u}|} \left[ -2[K_{1}] \frac{-[K_{2}]}{|C_{u}|} - [K_{3}] \frac{-[K_{2}]}{|C_{q}|} \right] \dot{\mathbf{q}}^{3} 
= \frac{1}{|C_{u}|} \left[ -2[K_{1}] \frac{-[K_{2}]}{|C_{u}|} - [K_{3}] \frac{-[K_{2}]}{|C_{q}|} \right] [\dot{\mathbf{u}} \dot{\mathbf{w}}]^{3} 
= \frac{1}{|C_{u}|} \left[ -2[K_{1}] \frac{-[K_{2}]}{|C_{u}|} - [K_{3}] \frac{-[K_{2}]}{|C_{q}|} \right] [K_{4}]^{3} \dot{\mathbf{w}}^{3}$$
(2.65)

where,

 $[K_{1,2,3,4}]$  is only dependent on the hardpoint according to Paper A

The dependency proof for the second order motion  $\ddot{\mathbf{u}}$  can be derived using a similar method. Since the matrices  $[C_u], [C_q], [K_1], [K_2], [K_3]$  and  $[K_4]$  only depend on hardpoints layout, it can be shown that  $\frac{\ddot{\mathbf{u}}}{\ddot{\mathbf{w}}^3}$  and  $\frac{\ddot{\mathbf{u}}}{\ddot{\mathbf{w}}^2}$  are constant values with given hardpoints. Since the control points and the links' orientations, which were introduced in section 2.1.3, can already be used to control the first order targets, the y coordinates of each inner point i and outer point i' can be used to control the second and the third order targets.

The problem can be treated as an optimization problem. The tuning parameters are the y coordinate of each inner and outer hardpoint. And the

optimization goal is to find these y coordinates, which give the correct second and third order motions calculated from second and third order targets. The model in Section 2.1.1.1 is used to construct the optimization. Figure 2.4 shows the optimized hardpoints B', B with given targets and a control point  $B^o$ .

In summary, the second and the third order targets can be controlled by the length of the support links and their exact positions. Together with the first order control method, all hardpoints are unique calculated using optimization.

Compliance reverse method From Equation 2.18, it is possible to get the motion ratios  $\hat{V}_O^i/v_i$  and  $\hat{\omega}_O^i/v_i$  for every input at i=A,B,C,D,E. Combining all these equations and allowing bushing deformation to be considered as the input, it is possible to calculate the contribution of each bushing on a particular compliance target. Considering brake steer  $\delta_A$  as the steer effect caused in the suspension system by the bushing at point A, it can be written as,

$$\delta_A = \frac{\omega_{Oz}}{v_A} \cdot S_A \tag{2.66}$$

The bushing deformation  $S_A$  can be written as  $S_A = F_A/K_A$ 

$$\delta_A = \frac{\omega_{Oz}}{v_A} \cdot \frac{F_A}{K_A} \tag{2.67}$$

$$\delta_A = \frac{\omega_{Oz}}{v_A} \cdot \frac{F_{px} \cdot F_A}{F_{px}} \cdot \frac{1}{K_A} \tag{2.68}$$

$$\frac{\delta_A}{F_{px}} = \frac{\omega_{Oz}}{v_A} \cdot \frac{F_A}{F_{px}} \cdot \frac{1}{K_A} \tag{2.69}$$

In the equation above it can be seen that the terms  $\omega_{Oz}/v_A$  and  $F_A/F_{px}$  are constant as they are the motion ratio and the corresponding force distribution ratio. The constant terms can be expressed as  $\omega_z^{BF}{}_A$  for brake force load case.

$$\frac{\delta_A}{F_{px}} = \frac{\omega_{zA}^{BF}}{K_A} \tag{2.70}$$

Similarly,

Wind-up stiffness:

$$\frac{\angle Oy_i}{F_{px}} = \frac{\omega_{yi}^{BF}}{K_i} \tag{2.71}$$

Lateral force steer:

$$\frac{\delta_i}{F_{py}} = \frac{\omega_{zi}^{LF}}{K_i} \tag{2.72}$$

Lateral force camber:

$$\frac{\gamma_i}{F_{py}} = \frac{\omega_{xi}^{LF}}{v_i} \tag{2.73}$$

where, i = A,B,C,D,E

For longitudinal compliance, the brake force input is considered to be acting directly at the wheel center. So, the term corresponding to moment generated at wheel center due to forces at tyre contact point can be ignored in the force distribution equations for this case. Longitudinal compliance:

$$\frac{X_i}{F_{Ox}} = \frac{V_{OXi}}{K_i} \tag{2.74}$$

The overall compliance target can be considered as the sum of the individual bushing contribution. So overall brake steer is calculated as,

$$\frac{\delta}{F_{px}} = \frac{\delta_A}{F_{px}} + \frac{\delta_B}{F_{px}} + \frac{\delta_C}{F_{px}} + \frac{\delta_D}{F_{px}} + \frac{\delta_E}{F_{px}}$$
 (2.75)

$$\frac{\delta}{F_{px}} = \frac{\omega_{ZA}^{BF}}{K_A} + \frac{\omega_{ZB}^{BF}}{K_B} + \frac{\omega_{ZC}^{BF}}{K_C} + \frac{\omega_{ZD}^{BF}}{K_D} + \frac{\omega_{ZE}^{BF}}{K_E}$$
(2.76)

Considering 5 compliance targets, 5 linear equations can be formed and from the given compliance target inputs, the bushing radial stiffness can be calculated by inverse matrix operation.

$$\begin{bmatrix} \omega_{ZA}^{BF} & \omega_{ZB}^{BF} & \omega_{ZC}^{BF} & \omega_{ZD}^{BF} & \omega_{ZE}^{BF} \\ V_{OX_A} & V_{OX_B} & V_{OX_C} & V_{OX_D} & V_{OX_E} \\ \omega_{YA}^{BF} & \omega_{YB}^{BF} & \omega_{YC}^{BF} & \omega_{YD}^{BF} & \omega_{YE}^{BF} \\ \omega_{ZA}^{LF} & \omega_{ZB}^{LF} & \omega_{ZC}^{LF} & \omega_{ZD}^{LF} & \omega_{XE}^{LF} \\ \omega_{XA}^{LF} & \omega_{XB}^{LF} & \omega_{XC}^{LF} & \omega_{XD}^{LF} & \omega_{XE}^{LF} \end{bmatrix} \cdot \begin{bmatrix} \frac{1}{K_A} \\ \frac{1}{K_B} \\ \frac{1}{K_C} \\ \frac{1}{K_D} \\ \frac{1}{K_E} \end{bmatrix} = \begin{bmatrix} \text{Brake steer} \\ \text{Longitudinal compliance} \\ \text{Wind up stiffness} \\ \text{Lateral force steer} \\ \text{Lateral force camber} \\ \text{(2.77)} \end{bmatrix}$$

## 2.2 Target setup using RL

The first part of the section introduces a method that generates a suspension property file attached to the vehicle model. The second part of the section introduces the RL agent that interacts with the simulation environment and proposes new suspension kinematics targets.

#### 2.2.1 Simulation environment

#### 2.2.1.1 Artificial suspension property file

The suspension property files use the targets for the curve-based steering subsystem for the front axle, and the curve-based suspension subsystem for the rear axle. For the front steering subsystem, 3D splines are used to capture the motion of the steering knuckle. For the rear axle, 2D splines are used to capture the motion of the non-steering knuckle. The motion includes steer at ground, camber angle, side view angle, X-coordinate variation, and Y-coordinate variation. The motion in the front axle depends on rack travel¹ and jounce travel. The motion in the rear axle only depends on jounce travel.

To get a proper motion file, the first step is to calculate the general motion from given suspension kinematics targets. The concept of general motions  $\dot{\mathbf{q}}$  is described in Paper A. The relation between the general motion and the suspension kinematics targets is described in Chapter 3.1.1 [43] for a front

 $<sup>^1</sup>$ Rack travel refers to the displacement of the steering rack in a rack-and-pinion steering system.

axle and section 3 from Paper A for a rear axle. At a given jounce position u, the targets are given by reading the target curve. For example, the target curve Bump Steer is shown in Equation 2.78.

Bump Steer
$$(u) = 1^{st}$$
Bump Steer $+ 2^{nd}$ Bump Steer $+ u + 3^{rd}$ Bump Steer $+ u^2$  (2.78)

For jounce motion, the general motion  $\dot{\mathbf{q}}$  can be solved by a symbolic solver from the given target at a specific jounce position according to the suspension jounce target. The second step is to integrate the general motion with a small time step  $\Delta t$  to get the next position  $\mathbf{q}_{t+1}$ . The targets for the new position  $\mathbf{q}_{t+1}$  can be read again from the target curve. The process is repeated until the end of the jounce travel. The motion file is generated by the motion  $\mathbf{q}$  at each jounce position. For the steering motion, the process is similar to the jounce motion. The steering motion file is generated by the motion  $\mathbf{q}$  at each rack travel or steering wheel angle. To formulate the suspension property file represented by 3D splines for the front steering subsystem, a superposition of the steering motion and the jounce motion is used. Figure 2.6 shows the process of generating artificial suspension property files.

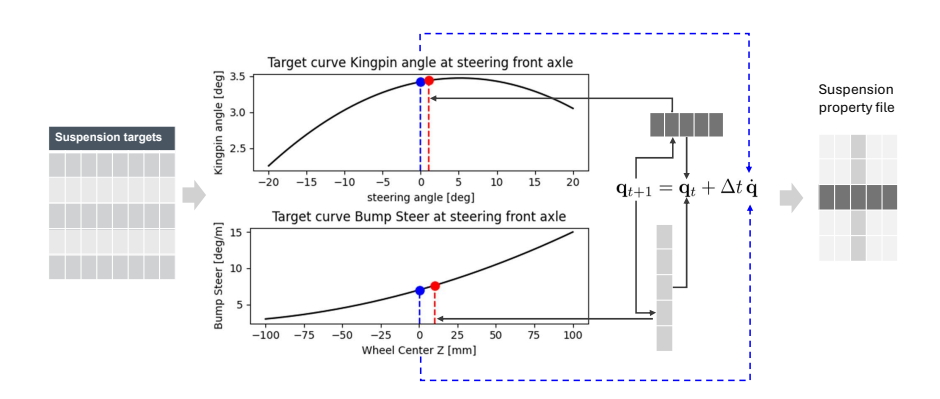


Figure 2.6. Generating artificial suspension property files

#### 2.2.1.2 RL environment

Once the suspension property files are generated, the RL environment shown in Figure 2.7 also includes a simulation environment [44], a reward function and a pre-check function. The mechanism of the pre-check function ensures that only the suspension property files that meet the target range can be simulated. Invalid suspension property files will lead to a punishment in the reward function. The shortcut path stabilizes the training process and improves training efficiency.

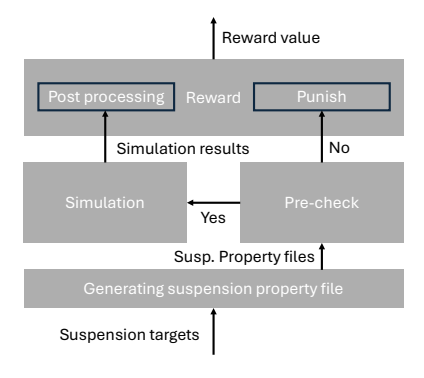


Figure 2.7. RL environment overview

Simulation scenarios The suspension property files are attached to an existing vehicle in this study. The vehicle is simulated in a set of driving scenarios, including acceleration, braking, and ramp steer events. The selected driving scenarios reflect the vehicle driving behaviors influenced by suspension kinematics targets. For example, the pitch angle during acceleration is influenced by the anti-lift in the front suspension and anti-squat in the rear suspension. The simulation scenarios aim to cover fundamental longitudinal and lateral vehicle dynamics behaviors. The measurement of the vehicle's performance is based on the extrapolated simulation results.

**Reward function** The reward function rewards the agent by comparing the simulation results and the target values. For each complete vehicle target i, it consists of complete vehicle target ranges  $[\epsilon_{min,i}, \epsilon_{max,i}]$ , maximum reward

 $R_{max,i}$ , and punishment gradient  $\dot{R}_i$ . The relation between the individual target reward  $R_i$  and the simulation result  $\epsilon_i$  is shown in Equation 2.79. If the suspension does not pass the pre-check in Figure 2.7, a punishment  $R_{punish,i}$  is assigned to the reward  $R_i$ .

$$R_{i} = \begin{cases} R_{max,i}, & \text{if } \epsilon_{min,i} < \epsilon_{i} < \epsilon_{max,i} \\ R_{max,i} - \dot{R}_{i} \cdot |\epsilon_{i} - \epsilon_{min,i}|, & \text{if } \epsilon_{i} < \epsilon_{min,i} \\ R_{max,i} - \dot{R}_{i} \cdot |\epsilon_{i} - \epsilon_{max,i}|, & \text{if } \epsilon_{i} > \epsilon_{max,i} \end{cases}$$

$$(2.79)$$

Equation 2.79 shows that the reward  $R_i$  is a linear function of the simulation result  $\epsilon_i$ . The reward  $R_i$  is set to  $R_{max,i}$  if the simulation result  $\epsilon_i$  is within the target range  $[\epsilon_{min,i}, \epsilon_{max,i}]$ . The reward  $R_i$  decreases linearly if the simulation result  $\epsilon_i$  is outside the target range. The total reward R is the summation of each individual reward  $R_i$  from Equation 2.79, meaning  $R = \sum_{i=1}^{n} R_i$ . The punishment gradient  $\dot{R}_i$  as weight factor is adjustable for different targets and learning tasks. The simulation environment is implemented in Python using the OpenAI Gym framework [45]. It cooperates with a learning agent to find the optimal suspension kinematics targets. The architecture of the learning agent is described in the next section.

### 2.2.2 Learning agent

The learning agent is adapted based on the stochastic Actor-Critic framework [46]. The actor part consists of multiple Gaussian distributions that represent the suspension kinematics targets. The critic part is modeled by a neural network function and outputs a high-dimensional value function that estimates the expected reward. The actor gets updated by the critic part using temporal-difference learning, and the critic part gets updated by training examples from the memory buffer. This section goes through the key elements and describes the learning mechanism of the learning agent.

#### 2.2.2.1 Agent critic

The critic neural network is used to estimate values  $\hat{\mathbf{V}}$  for individual suspension kinematics targets according to certain states shown in Figure 2.8. The weight vector  $\mathbb{W}$  includes scale weight w and bias term b. The states are

observations from the simulation environment. The critic neural network is implemented using PyTorch [47] with customized layers and sizes. To stabilize the training process, batch normalization is applied to the critic network. The gradient of each layer, which is used for training, is trimmed automatically based on the connections between layers. The critic neural network aims to generate values that update the policy in the actor part. A well-trained critic network should provide a good estimation of the expected reward, which leads to the convergence of the policy in the actor part.

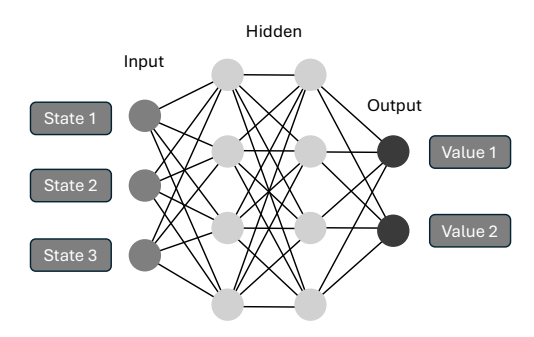


Figure 2.8. Critic network architecture

#### 2.2.2.2 Agent actor

The actor is supposed to generate suspension kinematics targets based on the policy. The policy  $\pi$  is a set of Gaussian distributions with mean  $\boldsymbol{\theta}_{u}^{\top}$  and standard deviation  $\theta_{\sigma}^{\top}$  as shown in Equation 2.80.

$$\pi(a|\boldsymbol{\theta}) = \frac{1}{\sqrt{2\pi\sigma(\boldsymbol{\theta})^2}} \exp\left(-\frac{(a-\mu(\boldsymbol{\theta}))^2}{2\sigma(\boldsymbol{\theta})^2}\right)$$
(2.80)

where:

$$a$$
 is the action

$$\mu(\boldsymbol{\theta}) = \boldsymbol{\theta}_{\mu}^{\scriptscriptstyle \perp}$$

$$\mu(\boldsymbol{\theta}) = \boldsymbol{\theta}_{\mu}^{\top}$$
$$\sigma(\boldsymbol{\theta}) = \boldsymbol{\theta}_{\sigma}^{\top}$$

To update the policy, the gradient with action a is expressed in Equations 2.81 and 2.82 from [46],

$$\nabla \ln \pi(a|\boldsymbol{\theta}_{\mu}) = \frac{1}{\sigma(\boldsymbol{\theta})^2} (a - \mu(\boldsymbol{\theta}))$$
 (2.81)

$$\nabla \ln \pi(a|\boldsymbol{\theta}_{\sigma}) = \frac{(a - \mu(\boldsymbol{\theta}))^2}{\sigma(\boldsymbol{\theta})^2} - 1$$
 (2.82)

#### 2.2.2.3 Training with Temporal-difference learning

The training process is based on the temporal-difference learning algorithm with average reward [48]. The temporal-difference  $\delta$  is a multi-dimensional scale vector that is broadcasted by one-dimensional reward and multi-dimensional predicted values, as shown in Equation 2.83.

$$\delta = \mathbf{R}_{t+1} - \bar{\mathbf{R}} + \hat{\mathbf{V}}(\mathbf{S}', \mathbb{W}) - \hat{\mathbf{V}}(\mathbf{S}, \mathbb{W})$$
(2.83)

where:

R and  $\bar{R}$  are one-dimensional scales reflecting total reward

 $\hat{m{V}}$  is a multi-dimensional vector from the critic network output

The weight update includes three steps for the average reward, critic, and actor parts. The average reward is updated by the temporal-difference  $\delta$  times the learning rate  $\alpha^{\bar{R}}$ . The gradient is essentially the key to weight updates together with the temporal-difference and learning rate. The gradient of the critic network can be obtained thanks to the PyTorch Autograd feature, and the actor part is calculated from Equations 2.81 and 2.82. The process of weight update is shown in Equations 2.84, 2.85, and 2.86.

$$\bar{R} \leftarrow \bar{R} + \alpha^{\bar{R}} \delta$$
 (2.84)

$$\mathbb{W} \leftarrow \mathbb{W} + \alpha^{\mathbb{W}} \boldsymbol{\delta} \nabla \hat{\boldsymbol{V}}(\boldsymbol{S}, \mathbb{W}) \tag{2.85}$$

$$\theta \leftarrow \theta + \alpha^{\theta} \delta \nabla \ln \pi(A|\theta)$$
 (2.86)

#### 2.2.2.4 Agent learning mechanism

The learning mechanism is shown in Figure 2.9 and Algorithm 1. The agent starts with an initial state, policy parameters  $\theta$ , and randomly initialized value

network parameters  $\mathbb{W}$ . The batch actions are sampled from the current policy distribution and fed into the simulation environment. The simulation experience is stored in the memory buffer. The action which has the highest reward will be used to update the actor weight factors. The experience in memory buffers is used to train the critic network with the help of the temporal-difference error shown in Equation 2.83. The memory buffer represents the historical experience. Notice that replay training with the memory buffer improves training efficiency. With the current state, a value can be estimated by the updated critic network and provide an updated TD-error. Then, the policy parameters  $\theta$  can be updated by the gradient of the policy from Equations 2.81 and 2.82. A clip function is applied to the policy parameters to avoid gradient explosion. If all actions generated by the policy fail to pass the pre-check function, the agent resets the state, average reward, and policy parameters. The agent repeats the process until the end of the training episode.

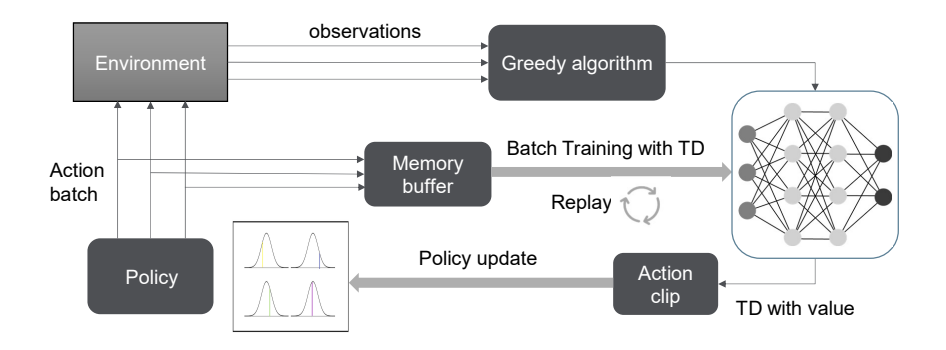


Figure 2.9. Agent learning mechanism

```
Algorithm 1 Agent learning algorithm based on Actor-Critic framework
   Initialize policy parameters \theta, value network parameters \mathbb{W}, initial state s_0,
   and initial average reward R
   Initialize learning rates \alpha_{\theta} and \alpha_{W} for actor and critic
   Initialize average reward learning rate \alpha^R
   for each of episode: do
       while All batch action A not pass Pre-check do
          Sample batch action A \sim \pi(\cdot|\theta) {Select action according to current
          policy}
          Execute action a_i \in A, observe reward r_i and next state s_i
          Store transition (s_i, a_i, r_i, s_i) in memory buffer
           while end of replay: do
              Sample the experience with batch size
              Compute TD error: \boldsymbol{\delta} = R - \bar{R} + \hat{\boldsymbol{V}}(S'|\mathbb{W}) - \hat{\boldsymbol{V}}(S|\mathbb{W}) \quad \{\boldsymbol{\delta} \in \mathbb{R}^s\}
              Update critic: \mathbb{W} \leftarrow \mathbb{W} + \alpha_w \, \boldsymbol{\delta} \, \nabla \hat{\boldsymbol{V}}(S, \mathbb{W})
          end while
          Select action a_{max} with the highest reward and update actor part with
           (s_{max}, a_{max}, r_{max}, s'_{max})
          Compute TD error: \hat{\boldsymbol{\delta}} = R - \bar{R} + \hat{\boldsymbol{V}}(S'|\mathbb{W}) - \hat{\boldsymbol{V}}(S|\mathbb{W}) \quad \{\boldsymbol{\delta} \in \mathbb{R}^s\}
          Update actor: \boldsymbol{\theta} \leftarrow \boldsymbol{\theta} + \alpha_{\boldsymbol{\theta}} I \boldsymbol{\delta} \nabla \ln \pi (a_{max} | \boldsymbol{\theta})
          Clip \theta_{\sigma} with interval [\theta_{\sigma}^{min}, \theta_{\sigma}^{max}]
          \bar{R} \leftarrow \bar{R} + \alpha^{\bar{R}} \, \delta_{max}
          I \leftarrow \gamma \, I
          s \leftarrow s'_{max}
       end while
      reset state s_0, average reward \bar{R}, and policy parameters \theta, I \leftarrow 1
```

end for

## CHAPTER 3

Case study

## **Chapter overview**

This chapter presents a comprehensive case study demonstrating the application of the proposed methodology. The investigation begins by establishing 14 complete vehicle targets, which serve as input for the reinforcement learning (RL) algorithm to determine the optimal 30 suspension targets as shown from vehicle level to subsystem level in Figure 3.1. Subsequently, a reverse kinematic algorithm (KDT) transforms these suspension targets into a feasible hardpoint configuration s shown from subsystem level to component level in Figure 3.1. For validation purposes, a simulatable suspension property file is generated from the derived hardpoints using VI-SuspensionGen. The complete vehicle targets are then simulated in VI-CarRealTime, enabling systematic verification that the design meets the specified performance criteria through compare shown in Figure 3.1. Furthermore, Figure 3.1 illustrates the case study workflow, which aligns with the 'V development process' depicted in Figure 1.1 with synthesize mindset. The KDT target phase (with blue rectangle) represents the progression from complete vehicle targets to suspension targets at the subsystem level, while the KDT suspension phase (with black rectangle) demonstrates the transition from suspension targets to hardpoints at the component level. Both levels undergo verification through artificial suspension property files as described in Section 2.2.1.1 and through VI-SuspensionGen. The outcomes of both the KDT target and KDT suspension phases are evaluated against the original target specifications.

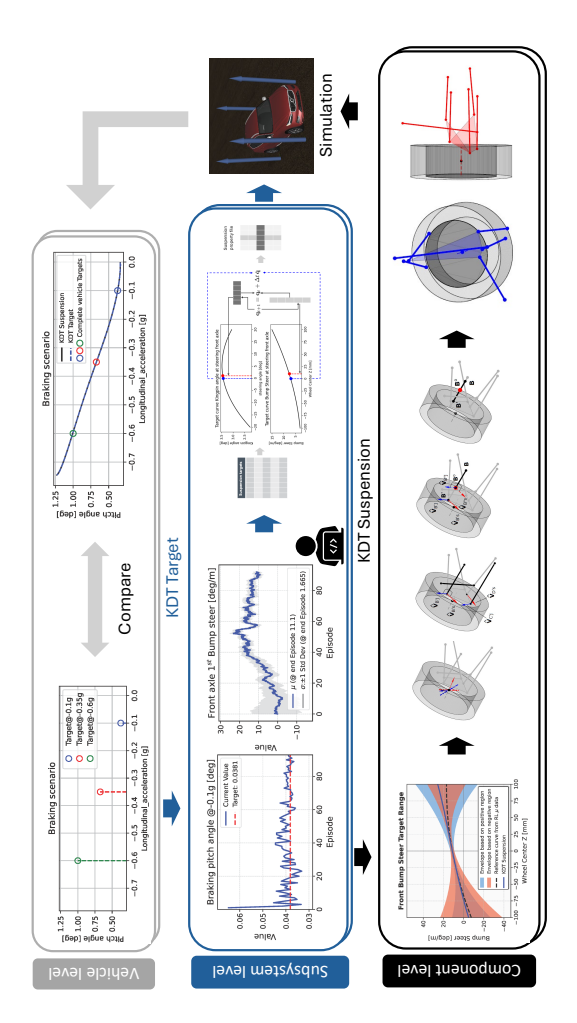


Figure 3.1. Case study flow overview aligned with the V development process

## 3.1 Complete vehicle target setup

Table 3.1 summarizes the selected complete vehicle targets across various driving scenarios. For acceleration and braking scenarios, pitch angles are measured at three distinct levels of longitudinal acceleration to capture the suspension kinematics during both minor and significant wheel travel. This approach specifically influences higher-order targets such as  $2^{nd}$  and  $3^{rd}$  Antilift coefficients. Roll motion is evaluated using a ramp steer scenario, with targets established for roll, pitch, and jacking motion. These parameters primarily influence kinematic targets like Roll Center Height (RCH). Additionally, understeer gradient is incorporated as a complete vehicle target to regulate suspension kinematics parameters, particularly Bump Steer and Bump Camber characteristics.

Table 3.1. Complete vehicle targets\*

Acceleration scenario	
Pitch angle @0.1g [deg] Pitch angle @0.5g	Pitch angle @0.35g
Braking scenario	
Pitch angle @-0.1g [deg] Pitch angle @-0.6g	Pitch angle @-0.35g
Ramp steer scenario for roll	
Roll angle @-0.2g [deg]	Roll angle @-0.5g
Ramp steer scenario for pitch	
Pitch angle @-0.2g [deg]	Pitch angle @-0.6g
Ramp steer scenario for Jacking	
Vertical displacement @-0.4g [mm]	Vertical displacement @-0.7g
Handling diagram from ramp steer	
Understeer gradient @0.1g [deg/g]	Understeer gradient @0.5g

<sup>\*</sup>These are example targets for a test vehicle used for the concept study at Volvo Cars.

This case study focuses on suspension targets related to jounce motion, as detailed in Table 3.3. Using the methodology outlined in Section 2.2, the primary objective is to determine the optimal suspension jounce targets that fulfill the complete vehicle requirements. To facilitate front suspension model that can be simulate, additional steering targets are listed as fixed parameters, as presented in Table 3.2.

The suspension kinematics targets outlined in Tables 3.3 and 3.2 are incorporated into the artificial suspension property file as described in Section 2.2.1.1. Subsequently, the algorithms detailed in Section 2.2.2.4 are applied to determine the optimal suspension targets from Table 3.3 that align vehicle performance most effectively with the complete vehicle targets specified in Table 3.1.

Table 3.2. Steering targets for the front suspension

First order	Second order	Third order	
Front suspension steering target			
1 <sup>st</sup> Caster angle	$2^{nd}$ Caster angle	$3^{rd}$ Caster angle	
[deg]	$[\deg/25\deg]$	$[\deg/25\deg^2]$	
1 <sup>st</sup> Kingpin angle	$2^{nd}$ Kingpin angle	$3^{rd}$ Kingpin angle	
[deg]	$[\deg/25\deg]$	$[\deg/25\deg^2]$	
$1^{st}$ Caster trail	$2^{nd}$ Caster trail	$3^{rd}$ Caster trail	
[mm]	[mm/25deg]	$[\mathrm{mm}/25\mathrm{deg^2}]$	
1 <sup>st</sup> Scrub radius	$2^{nd}$ Scrub radius	$3^{rd}$ Scrub radius	
[mm]	[mm/25deg]	$[mm/25deg^2]$	
$1^{st}$ WLLA	$2^{nd}$ WLLA	$3^{rd}$ WLLA	
[mm]	[mm/25deg]	$[\mathrm{mm}/25\mathrm{deg}^2]$	
Front suspension steering geometry target			
$\delta_L \text{ [deg]}$	$\delta_R \; [\mathrm{deg}]$	$R_s \text{ [mm]}$	

WLLA: Wheel load level arm

 $\delta_L \colon$  Maximum steering angle to the left

 $\delta_R \colon$  Maximum steering angle to the right

 $R_s$ : Maximum rack travel

Table 3.3. Jounce targets selected to generate suspension property file

First order	Second order	Third order
Front suspension jo	ounce target	
$1^{st}$ Bump Steer	2 <sup>nd</sup> Bump Steer	3 <sup>rd</sup> Bump Steer
$[\deg/m]$	[(deg/m)/dm]	$[(deg/m)/dm^2]$
$1^{st}$ Bump Camber	$2^{nd}$ Bump Camber	$3^{rd}$ Bump Camber
[deg/m]	[(deg/m)/dm]	$[(deg/m)/dm^2]$
$1^{st}$ Anti-dive	$2^{nd}$ Anti-dive	$3^{rd}$ Anti-dive
[%]	[%/dm]	$[\%/\mathrm{dm}^2]$
1 <sup>st</sup> Anti-lift	$2^{nd}$ Anti-lift	$3^{rd}$ Anti-lift
[%]	[%/dm]	$[\%/\mathrm{dm}^2]$
$1^{st}$ RCH	$2^{nd}$ RCH	$3^{rd}$ RCH
[mm]	$[\mathrm{mm/dm}]$	$[\mathrm{mm}/\mathrm{dm}^2]$
Rear suspension jo	unce target	
$1^{st}$ Bump Steer	$2^{nd}$ Bump Steer	3 <sup>rd</sup> Bump Steer
[deg/m]	[(deg/m)/dm]	$[(deg/m)/dm^2]$
$1^{st}$ Bump Camber	$2^{nd}$ Bump Camber	$3^{rd}$ Bump Camber
$[\deg/m]$	[(deg/m)/dm]	$[(\mathrm{deg/m})/\mathrm{dm}^2]$
$1^{st}$ Anti-squat	$2^{nd}$ Anti-squat	$3^{rd}$ Anti-squat
[%]	$[\%/\mathrm{dm}]$	$[\%/\mathrm{dm^2}]$
1 <sup>st</sup> Anti-lift	$2^{nd}$ Anti-lift	$3^{rd}$ Anti-lift
[%]	$[\%/\mathrm{dm}]$	$[[\%/\mathrm{dm}^2]$
$1^{st}$ RCH	$2^{nd}$ RCH	$3^{rd}$ RCH
[mm]	[mm/dm]	$[\mathrm{mm}/\mathrm{dm}^2]$

## 3.2 RL learning process

Figure 3.2 illustrates the training progression, depicting the best reward achieved per episode. The learning curve exhibits both rapid advancement phases and periods of incremental improvement. The training process concluded at episode 93, reaching an optimal reward value of -83. This termination threshold was established based on comprehensive experimental validation. For this case study, the early stopping criteria also play a role in preventing overfitting.

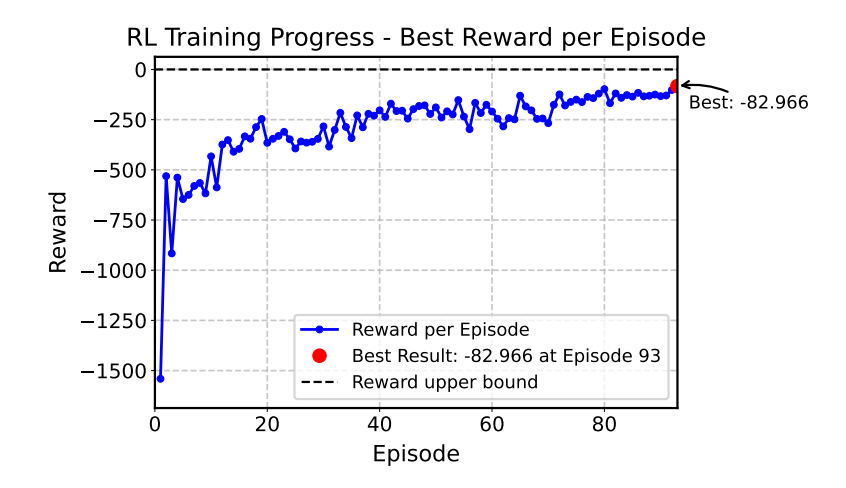


Figure 3.2. Reward for each episode during the RL training process

Figure 3.3 illustrates the learning progression for each individual complete vehicle target. Throughout the training process, the reinforcement learning agent effectively balances these multiple targets, achieving convergence by the final episode. The convergence characteristics of the suspension targets will be examined in detail in the following section.

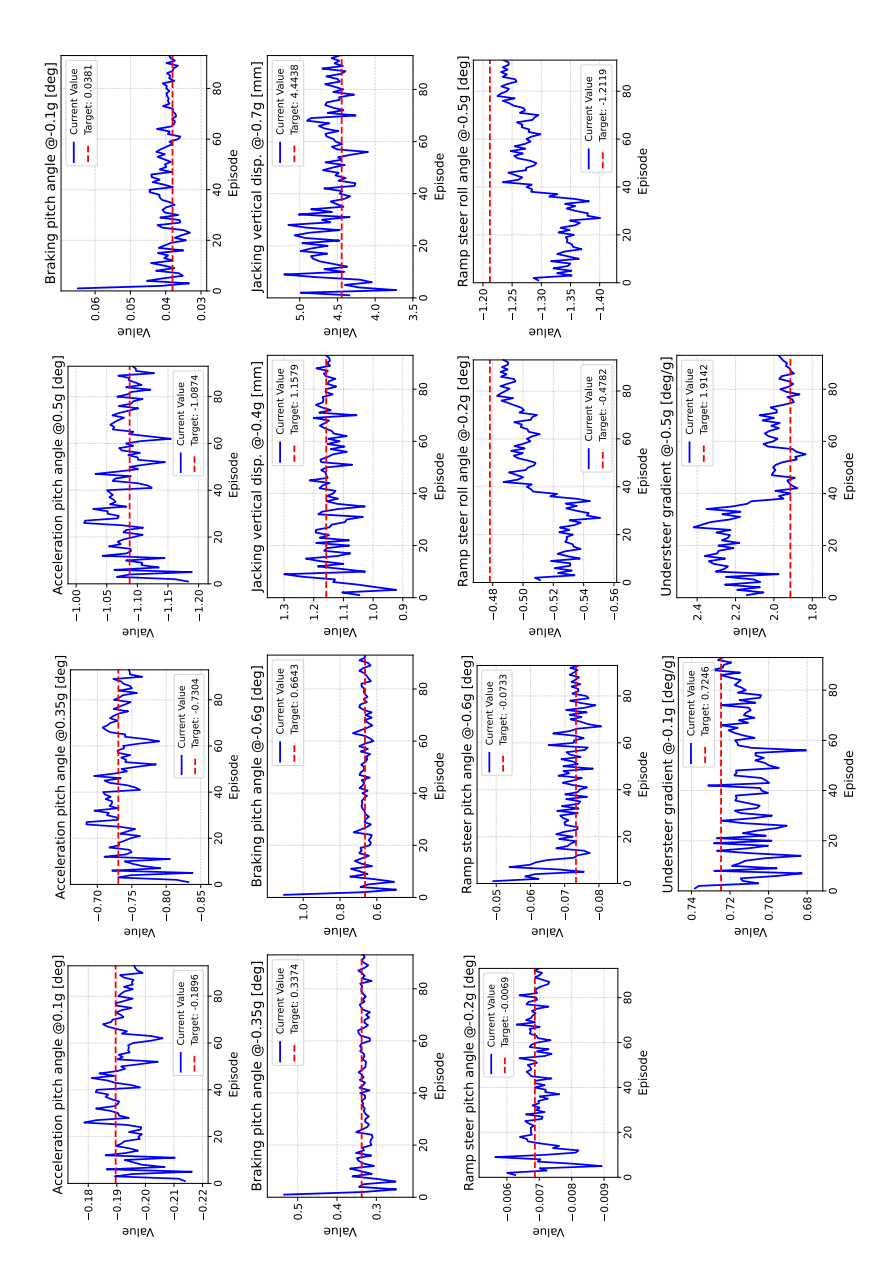
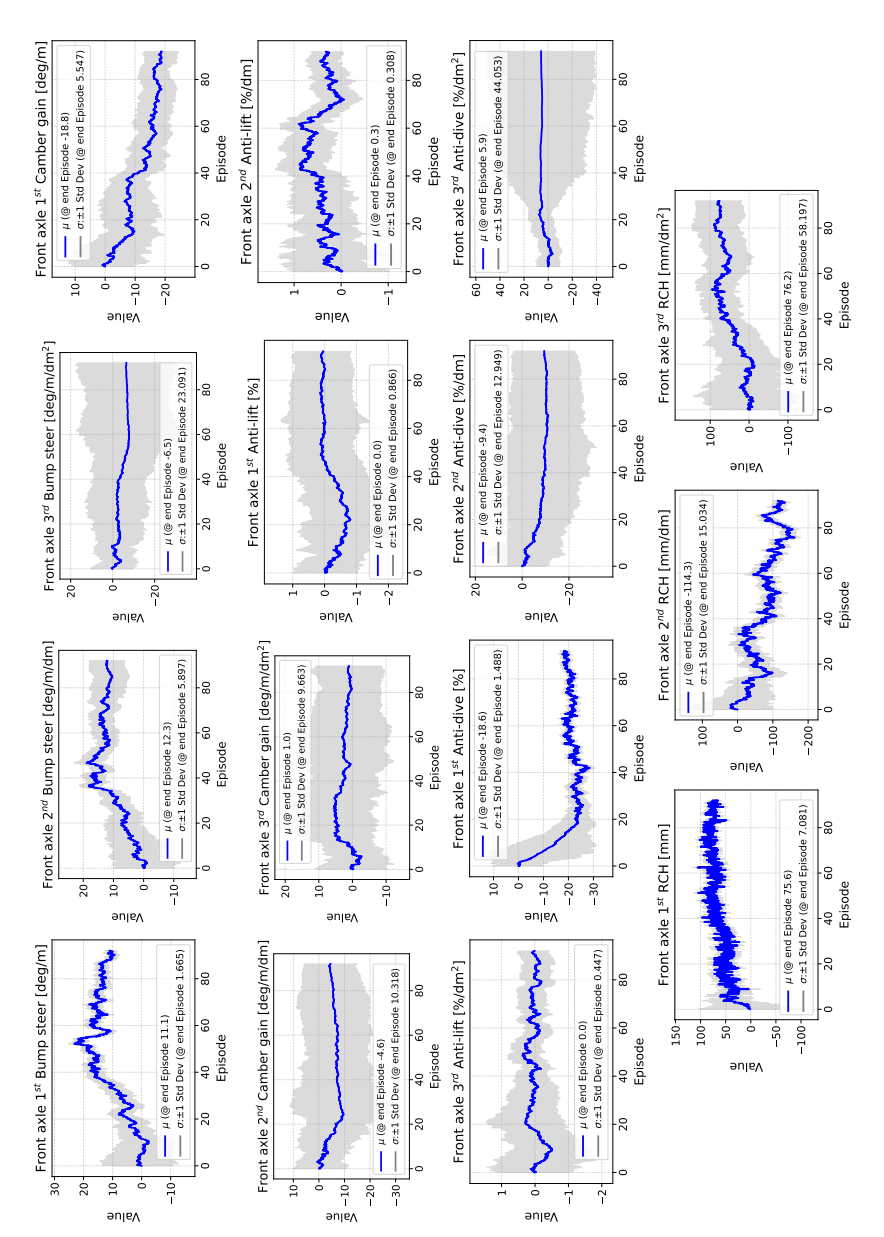


Figure 3.3. Learning curve per episode: Individual complete vehicle target learning process

## 3.3 Learning curve for suspension targets

In alignment with the complete vehicle target learning curve illustrated in Figure 3.3, the suspension target learning process is characterized by two key parameters: mean  $\mu$  and standard deviation  $\sigma$  per episode, as shown in Figures 3.4 and 3.5. These parameters correspond to the policy parameters defined in Equation 2.80. While some subfigures demonstrate convergence of both the mean value and its variation, others exhibit only partial convergence. As established in Equation 2.78, the nonlinear suspension target incorporates coefficients up to the third order. Consequently, the learning outcomes for each coefficient, expressed in terms of  $\mu$  and  $\sigma$ , must be transformed into a comprehensive target range that accounts for their nonlinear interdependencies. The methodology for this transformation will be detailed in the following section.



**Figure 3.4.** Learning curve per episode with  $\mu$  and  $\sigma$  for front axle suspension targets

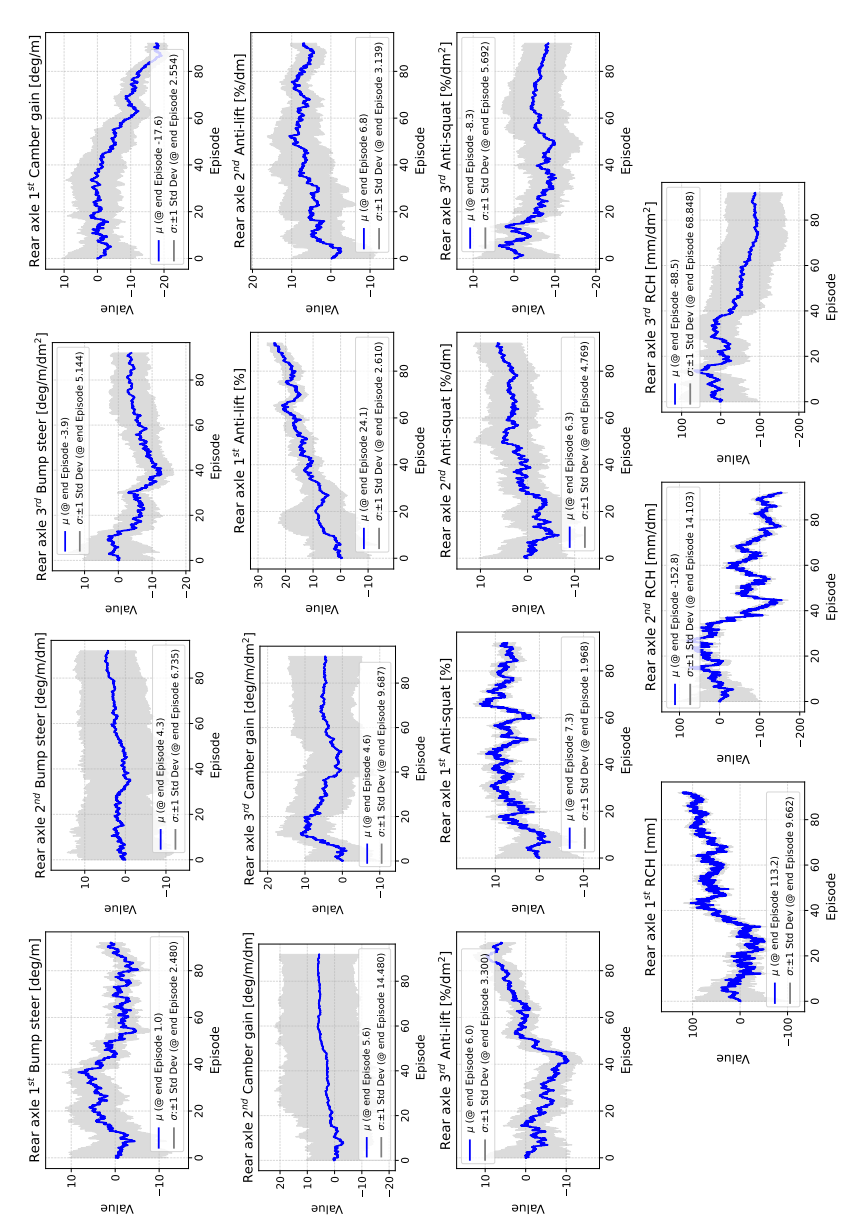


Figure 3.5. Learning curve per episode with  $\mu$  and  $\sigma$  Rear axle

# 3.4 Suspension target representation (KDT Target)

Section 3.3 outputs suspension targets as mean  $(\mu)$  ± standard deviation  $(\sigma)$  up to third order. The hardpoint are not fully specified by the suspension targets. We will use the control point 2.1.3 to fullfill the additional wishes, such as geometrical packaging constraints. To facilitate the suspension hardpoint design process, a comprehensive envelope encompassing all viable coefficient combinations is essential. Algorithm 2 transforms these statistical parameters  $(\mu \text{ and } \sigma)$  shown in Figures 3.4 and 3.5 into the boundary envelopes presented in Figure 3.6. To maintain coefficient consistency across both positive and negative wheel travel regions, the Polynomial Coefficient Envelope algorithm initially identifies the coefficient set that maximizes the envelope area in the positive wheel travel region. These identified coefficients are then extend to the negative region to ensure coefficient continuity. Similarly, the algorithm determines a second set of coefficients that maximize the envelope area in the negative wheel travel region and extends them to the positive region. Consequently, each target is bounded by two distinct envelopes representing the coefficient sets optimized for the positive and negative wheel travel regions respectively.

Figure 3.6 illustrates the target envelopes comprising both positive and negative wheel travel regions, along with the reference curve derived from the mean  $(\mu)$  values obtained through reinforcement learning. These envelopes establish the design constraints for the subsequent hardpoint configuration process. The primary objective is to ensure that the actual suspension kinematic performance, denoted as KDT suspension in Figure 3.6, remains within at least one of the envelope boundaries, either in the positive (blue shaded) or negative (red shaded) wheel travel region.

#### Algorithm 2 Polynomial Coefficient Envelope algorithm

```
Require: 1^{st}\mu, 2^{nd}\mu, 3^{rd}\mu, 1^{st}\sigma, 2^{nd}\sigma, 3^{rd}\sigma
Ensure: Coefficient combinations for envelopes
  combinations \leftarrow \{\} {Generate all possible coefficient combinations}
  for a \in \{1^{st}\mu - 1^{st}\sigma, 1^{st}\mu + 1^{st}\sigma\} do
     for b \in \{2^{nd}\mu - 2^{nd}\sigma, 2^{nd}\mu + 2^{nd}\sigma\} do
       for c \in \{3^{rd}\mu - 3^{rd}\sigma, 3^{rd}\mu + 3^{rd}\sigma\} do
          Add (a, b, c) to combinations
        end for
     end for
  end for
  Initialize pos max area \leftarrow -\infty, pos min area \leftarrow +\infty
  Initialize neg \ max \ area \leftarrow -\infty, neg \ min \ area \leftarrow +\infty
  for each combo \in combinations do
     pos \ area \leftarrow \sum polynomial(x \ pos, combo) \{Evaluate in positive region\}
     if pos \ area > pos \ max \ area then
        pos \ max \ area \leftarrow pos \ area
     end if
     if pos area < pos min area then
       pos min area \leftarrow pos area
     end if
     neg\_area \leftarrow \sum polynomial(x\_neg, combo) {Evaluate in negative re-
     if neg\_area > neg\_max\_area then
        neg max area \leftarrow neg area
     end if
     if neg\_area < neg\_min\_area then
        neq min area \leftarrow neq area
     end if
  end for
  return pos max area, pos min area,
              neg max area, neg_min_area {These define the upper and
  lower envelope boundaries}
```

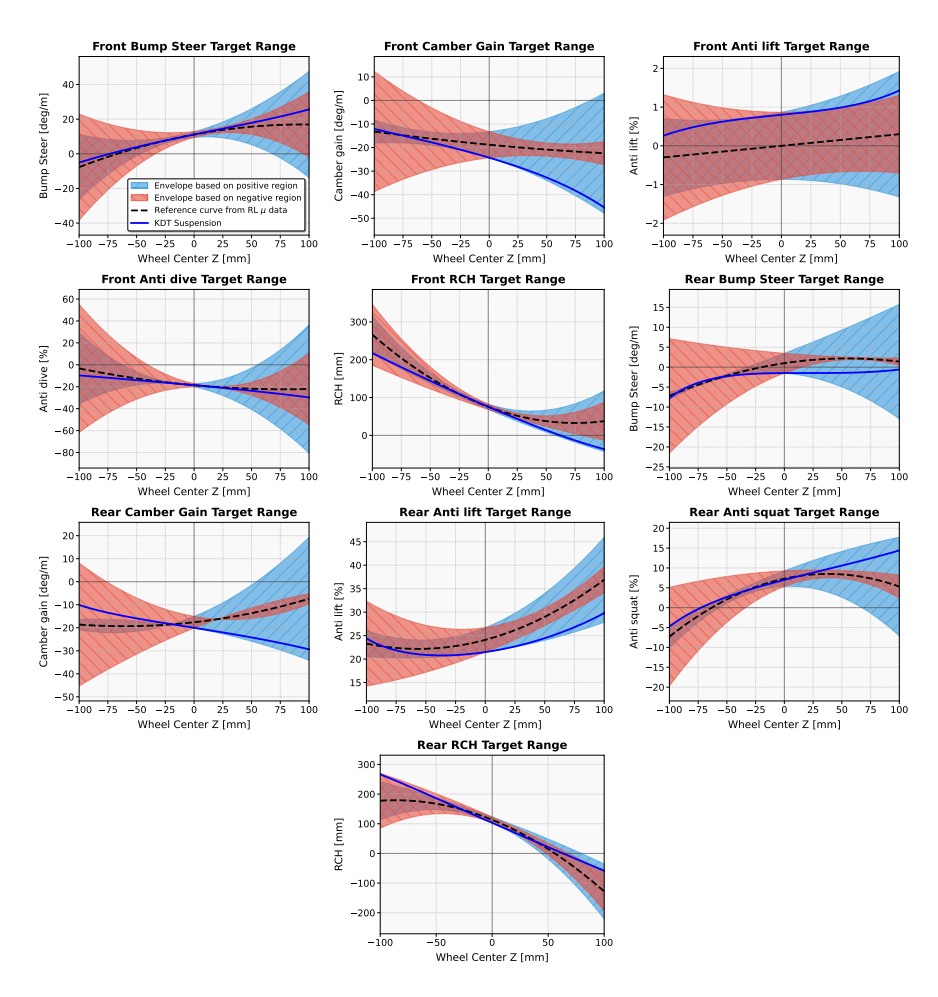


Figure 3.6. Suspension target representation (KDT target): Target envelopes with positive and negative regions

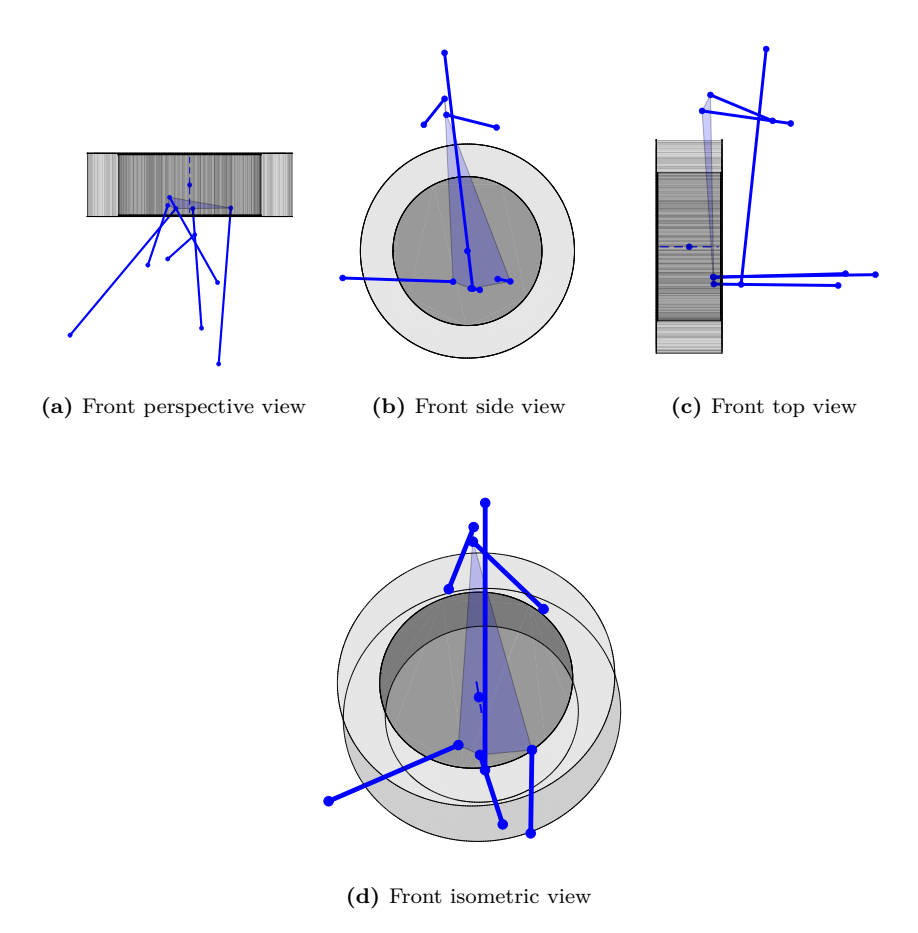
## 3.5 Hardpoint setup (KDT Suspension)

The hardpoint design applies Section 2.1.3's methodology to the targets in Tables 3.3-3.2 and parameters from Figures 3.4-3.5. This design process strategically balances packaging constraints and performance requirements within the envelope constraints discussed in Section 3.4. The resulting hardpoint configuration exhibits only minor deviations from the Rear Camber gain target. Figures 3.7 and 3.8 illustrate the hardpoint configurations for the front and rear axles, respectively. The actual kinematic performance of this configuration is represented by the blue line labeled "KDT suspension" in Figure 3.6. Notably, the actual camber gain slightly exceeds the target envelope during significant rebound travel. This deviation exemplifies a fundamental limitation of the artificial suspension concept described in Section 2.2.1.1, which does not inherently account for physical packaging constraints. Nevertheless, the AI-supported algorithms significantly reduce the design iteration time while effectively optimizing both packaging feasibility and kinematic performance criteria.

With the established hardpoint configuration, VI-SuspensionGen generates a comprehensive suspension property file for VI-CarRealTime simulations. These simulation results provide critical validation by enabling direct comparison against the original target specifications. The following section presents a detailed comparison between the initial target parameters and the simulation outcomes from the actual suspension design implemented through the proposed methodology.

## 3.6 Closing the design loop

Figure 3.9 demonstrates that both the target learning algorithm and hard-point design algorithms effectively achieved their intended purposes. The verification focuses on comparing the performance against the original targets established in Table 3.1. The blue dashed line (KDT\_Target) represents the artificial suspension model with optimized kinematic targets before hardpoint implementation, while the black solid line (KDT\_Suspension) represents the performance of the actual hardpoint configuration. This comparison confirms the successful translation from vehicle-level targets to physical suspension geometry.



 $\textbf{\textit{Figure 3.7.}} \ \ \textit{Front suspension hardpoint configuration showing different viewing angles}$ 

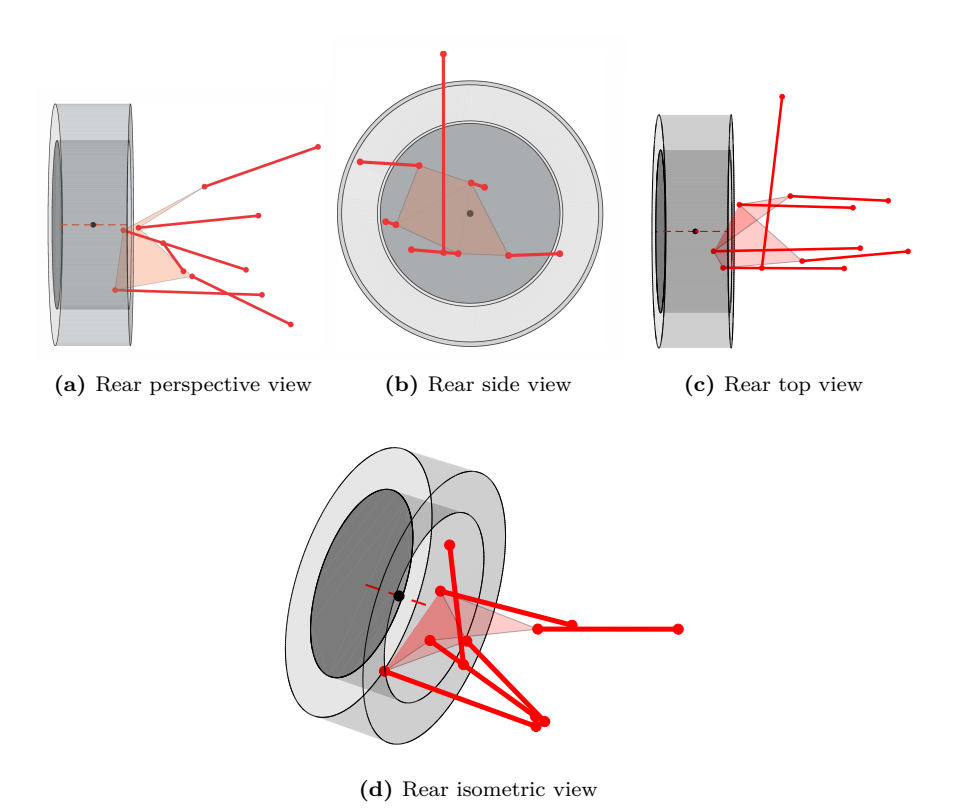


Figure 3.8. Rear suspension hardpoint configuration showing different viewing angles

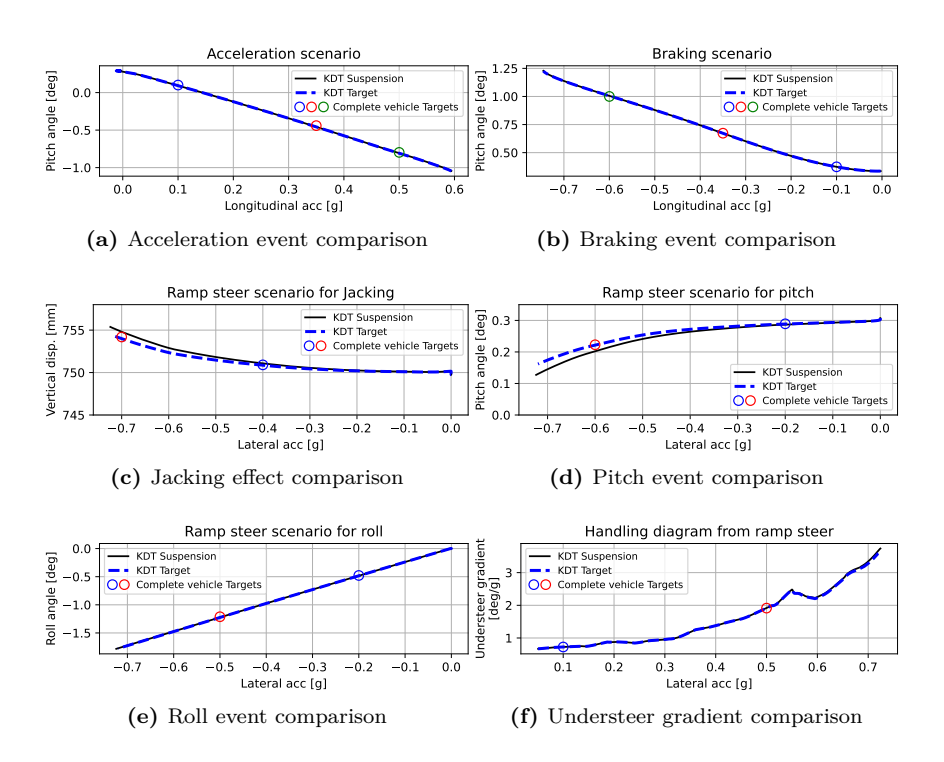


Figure 3.9. Comparison of original targets with simulation results from actual suspension design

# 3.7 Summary

This chapter has demonstrated the complete design workflow from vehicle targets to suspension hardpoints. The process began with 14 complete vehicle targets that were used by the reinforcement learning algorithm to establish 30 suspension kinematic targets. Additionally, some fixed values were given, such as vehicle data and some fixed suspension parameters, e.g., wheel rate, which was not allowed to vary in the design. These suspension targets guided the hardpoint configuration using the KDT algorithm.

Key findings from this case study include:

- The reinforcement learning algorithm effectively converged on optimal suspension targets that fulfilled the specified complete vehicle performance requirements
- The kinematic reverse design (KDT) algorithm successfully transformed the abstract suspension targets into a physically feasible hardpoint configuration, exhibiting only minimal deviation in rear camber gain characteristics
- The implemented design demonstrated excellent correlation with the original vehicle targets across all evaluated performance metrics
- The automated methodology substantially reduced the design iteration cycle while maintaining precise adherence to performance specifications

This case study provides validation of the methodology described in Chapters 1 and 2, demonstrating its robustness and practical efficacy in real-world automotive suspension design applications. The results confirm that the proposed approach successfully bridges the gap between theoretical vehicle dynamics targets and physically implementable suspension geometries.

# CHAPTER 4

Conclusion

This chapter synthesizes the key findings, discusses their broader implications, and outlines future research directions that emerge from this work.

# 4.1 Summary of research contributions

This thesis has developed a comprehensive AI-supported framework for road vehicle suspension design that transforms the traditional development process. By reversing the conventional design flow, from component-level design to performance verification, this research has established methodologies that efficiently derive suspension solutions directly from vehicle-level requirements. The integrated approach consists of two major innovations:

First, a reinforcement learning framework efficiently translates complete vehicle targets into specific suspension kinematics targets, effectively navigating the complex, high-dimensional design space that has traditionally challenged optimization approaches. This methodology demonstrates superior convergence properties and accuracy, largely due to its ability to accumulate experiential knowledge through environmental interactions and mirroring the learning process of human experts.

Second, a reverse engineering methodology transforms these suspension targets into precise hardpoint configurations and bushing specifications. This automated translation eliminates conventional trial-and-error processes, providing suspension engineers with clear design guidelines that simultaneously satisfy performance requirements and packaging constraints. The mathematical foundation ensures unique correlations between performance targets and physical implementations, enabling engineers to build clear connections between performance expectations and design parameters.

The case study presented in Chapter 3 validates the practical effectiveness of this integrated methodology. The reinforcement learning algorithm successfully derived 30 suspension kinematic targets from 14 complete vehicle targets, which were subsequently translated into viable hardpoint configurations through the KDT algorithm. The resulting design demonstrated excellent concordance with the original vehicle targets, with only minor deviations in specific parameters.

# 4.2 Significance and impact

The significance of this research extends beyond its methodological contributions to encompass substantial practical benefits for automotive development. This work bridges the theoretical-practical divide by transforming abstract vehicle dynamics principles into implementable design frameworks. The innovations presented not only advance the academic understanding of suspension design but also address critical industry challenges related to development efficiency, product performance, and organizational collaboration. By providing a systematic approach to translate vehicle-level requirements directly into physical design parameters, this research fundamentally restructures the suspension development workflow, allowing manufacturers to respond more effectively to rapidly evolving market demands while maintaining engineering excellence. The practical implications manifest across multiple dimensions of the automotive development ecosystem, see the following sections.

# 4.2.1 Efficiency enhancements

The framework developed in this research cuts development time by approximately 50%, as shown in the papers. This significant time saving is vital in

today's automotive industry. Car manufacturers face growing pressure from electrification demands and global competition. The new methodology automates complex design calculations that previously required extensive manual effort. It eliminates the need for repeated simulation cycles that traditionally consumed substantial engineering resources. Engineers can now test many more design alternatives in a shorter timeframe. This efficiency allows design teams to explore a wider range of solutions while meeting increasingly tight project deadlines. The time saved can be redirected to other critical development activities or used to further refine suspension designs. For automotive companies operating in competitive markets, this acceleration of the design process that provides competitive advantage.

#### 4.2.2 Cross-functional collaboration

The methodology significantly enhances cross-departmental collaboration by establishing a shared technical language. Vehicle dynamics engineers focus on defining vehicle behavior requirements, while design engineers concentrate on packaging constraints. Traditionally, these specialized groups have struggled to communicate effectively due to their differing technical perspectives. The framework presented in this thesis bridges this communication gap.

The system automatically converts performance requirements into specific geometry constraints. These constraints are clear and precise. Packaging engineers receive exact boundaries for their design work. Vehicle dynamics engineers can clearly express their needs in terms that directly guide physical design.

This shared understanding reduces conflicts between departments. It eliminates the back-and-forth iterations that waste time in traditional processes. Teams can work in parallel with confidence. The design engineers know they are working within the right parameters. The vehicle dynamics engineers can trust that their performance targets will be met. This collaborative approach fosters a more efficient development environment.

# 4.2.3 Improved design quality

The methodologies developed in this research enhance the quality of suspension designs. By automating the translation of performance targets into hard-point configurations, the framework minimizes human error and subjective

interpretation. The mathematical relationships established between vehicle-level requirements and component specifications ensure that designs are not only feasible but also optimized for performance. This leads to more consistent and reliable suspension systems that meet or exceed performance expectations. The ability to explore a wider range of design alternatives also contributes to improved design quality, as engineers can evaluate multiple configurations and select the most effective solutions.

#### 4.2.4 Balance between AI and human expertise

The framework developed in this research establishes a balanced relationship between artificial intelligence and human engineering expertise. Rather than attempting to replace human judgment, the AI methodologies serve as sophisticated tools that augment the capabilities of suspension engineers. The reinforcement learning algorithm handles the computationally intensive exploration of the design space while engineers run the reverse engineering process to derive hardpoint configurations with packaging constraints.

This balanced approach acknowledges that effective suspension design requires both quantitative optimization and qualitative engineering judgment. The AI components manage the mathematical complexity of translating vehicle-level requirements into component specifications, freeing engineers to focus on higher-level considerations such as vehicle character, brand DNA, and subjective performance qualities that remain difficult to fully quantify. By automating routine calculations and parameter correlations, the framework allows engineers to devote more attention to innovative solutions and edge cases that benefit from human creativity and experience.

Meanwhile, the system maintains transparency in its operations, allowing engineers to understand and trace the AI's learning process. This transparency builds trust in the automated components while simultaneously creating educational opportunities for junior engineers to observe the systematic relationships between design decisions and performance outcomes. The result is a symbiotic relationship where AI handles the computational burden while engineers apply contextual understanding and domain expertise to guide and refine the process.

#### 4.2.5 Holistic system understanding

By establishing clear mathematical relationships between vehicle-level requirements, suspension targets, and component specifications, the research enhances system understanding across organizational hierarchies. This comprehensive view enables more effective requirement management and system-level optimization throughout the development process.

The framework creates a traceable path from customer-oriented performance metrics to specific engineering parameters, illuminating previously obscured correlations in the complex suspension system. This traceability serves both educational and practical purposes—junior engineers can quickly grasp system interdependencies that traditionally required years of experience to internalize, while senior engineers gain quantitative validation for their experiential knowledge.

Furthermore, the mathematical formalization transforms what was once predominantly tacit knowledge into explicit, documented understanding. This codification of suspension design principles creates organizational resilience by reducing dependency on individual expertise and establishing a foundation for continuous improvement. The quantifiable relationships between design decisions and performance outcomes also facilitate more objective communication with non-technical stakeholders, improving alignment between engineering teams and broader business objectives.

Most significantly, this holistic framework enables engineers to anticipate the cascading effects of design changes across the vehicle system. When modifications become necessary due to packaging constraints or other requirements, the impact on vehicle performance can be immediately assessed without extensive simulation cycles, allowing for more agile and informed decision-making throughout the development process.

### 4.3 Limitations and future research directions

This thesis has important limitations that should be addressed. These limitations are not just constraints. They are opportunities for future research. Our methods work well within their scope. Yet they face several theoretical and practical limits. These limits come from simplified models, computing constraints, and our focused research goals. The sections below describe these limitations. They also outline promising research directions. Future re-

searchers can build on our work by addressing these opportunities. This will expand both the theory and practice of AI-supported suspension design:

#### 4.3.1 Scope expansion

The current methodology primarily addresses longitudinal and lateral dynamics, with limited consideration of vertical dynamics and ride comfort. Future research should extend the framework to incorporate additional subsystems such as springs, dampers, and particularly tyres, creating a more comprehensive approach to suspension design that addresses all primary vehicle dynamics domains.

The inclusion of tyre dynamics represents an especially critical extension. Tyres constitute the sole contact point between vehicle and road, functioning as the fundamental medium through which all suspension forces are ultimately transmitted. The current framework treats tire behavior in as fixed model without parameterization, which simplifies the design process. Future work should integrate sophisticated tire models that capture these nonlinearities, including load sensitivity, combined slip conditions, and transient behavior.

Moreover, the interconnected nature of tire-suspension dynamics creates a coupled optimization problem that cannot be fully addressed through sequential design approaches. A comprehensive framework would consider how suspension geometry affects dynamic tire loading, and conversely, how tire characteristics influence optimal suspension response. This bi-directional relationship necessitates simultaneous optimization of both systems, potentially through reinforcement learning algorithms capable of navigating this expanded design space.

# 4.3.2 Integration of compliance and kinematics

While the thesis presents methodologies for both kinematics and compliance design, these approaches are not fully integrated within a unified optimization framework. Developing a reinforcement learning approach that simultaneously optimizes kinematics and compliance targets would yield more balanced designs that better reflect real-world performance requirements. The current sequential approach—optimizing kinematics first, followed by compliance—cannot capture the complex interdependencies between these domains. Future research should focus on creating a holistic optimization framework

where the agent can learn to balance trade-offs between kinematic and compliance characteristics in a single design process. Such integration would better reflect the physical reality of suspension systems, where kinematic motion and compliant deformation occur simultaneously rather than independently. This approach could potentially uncover novel design solutions that are overlooked when these domains are treated separately, particularly for vehicles with demanding performance requirements across multiple operating conditions.

#### 4.3.3 Nonlinear compliance behavior

The compliance methodology focuses exclusively on linear behavior, whereas real-world suspension systems often exhibit significant non-linearities of the design variables, particularly under large articulations. Extending the KDT algorithm to incorporate nonlinear bushing behavior would enhance the fidelity of the compliance design process.

The current linear approximation works well within limited operating ranges but becomes increasingly inaccurate as suspension systems experience larger displacements and forces. Real automotive bushings typically demonstrate progressive stiffness characteristics. Initially compliant to absorb minor disturbances but becoming progressively stiffer to maintain stability under extreme conditions. This nonlinear behavior serves crucial functions: it provides ride comfort during normal driving while ensuring robust handling during emergency maneuvers or when carrying varying loads.

From a mathematical perspective, incorporating these nonlinearities presents significant challenges. The KDT algorithm would need to evolve from simple stiffness matrices to more sophisticated representations capable of capturing hysteresis loops, progressive rate functions, and coupled directional effects. This would require developing inverse modeling techniques that can derive nonlinear bushing specifications from desired force-displacement characteristics across the entire operating range.

# 4.3.4 Transfer learning and knowledge reuse

The current methodology requires training reinforcement learning agents from scratch for each new vehicle program, which is computationally expensive and time-consuming. A significant opportunity exists in developing robust transfer learning capabilities that leverage knowledge across different vehicle

platforms and suspension configurations. Pre-trained models could capture fundamental suspension physics and design principles that remain consistent across vehicles, dramatically accelerating the optimization process for new applications.

Transfer learning in this context would involve identifying invariant relationships between design parameters and performance outcomes that transcend specific vehicle characteristics such as mass, wheelbase, or target market. For example, the fundamental influence of roll center height on body roll behavior follows consistent physical principles regardless of vehicle type. An agent trained on sedan suspension dynamics could transfer this knowledge when designing SUV suspensions, requiring only fine-tuning rather than complete retraining.

Several promising research directions emerge from this limitation. First, developing modular learning architectures that separate vehicle-specific knowledge from universal suspension principles would enable more effective knowledge transfer. Second, meta-learning approaches could be investigated to develop agents that "learn how to learn" suspension design, becoming progressively more efficient with each new vehicle program. Third, knowledge distillation techniques could compress insights from multiple vehicle designs into compact, transferable models that serve as starting points for new optimization problems.

The potential benefits extend beyond computational efficiency. Transfer learning could capture tacit engineering knowledge that might otherwise be lost during organizational changes or retirements. It could also facilitate cross-platform standardization by identifying common design patterns that work well across multiple vehicle types, potentially reducing manufacturing complexity while maintaining performance differentiation. Furthermore, a transfer learning framework would create a systematic mechanism for continuous organizational learning, where each completed vehicle design enriches the knowledge base for future projects.

# 4.4 Concluding remarks

In conclusion, this thesis has established a robust foundation for AI-supported suspension design that significantly enhances both efficiency and precision in automotive development. The methodologies developed demonstrate the potential to revolutionize suspension development, particularly during the critical concept phase. By transforming the conventional design process from a component-to-performance approach to a performance-to-component methodology, this research enables engineers to establish comprehensive vehicle-level targets without immediate concern for construction details or system feasibility.

The 50% reduction in lead time and improved precision demonstrate the framework's potential for industrial adoption. As the industry continues to navigate transitions toward electrification and autonomous driving technologies, such efficiency gains in foundational mechanical systems like suspension design become increasingly valuable. The frameworks established in this thesis not only address immediate engineering challenges but also provide a template for how AI methodologies can be effectively integrated into complex engineering domains where human expertise remains indispensable.

#### References

- [1] Bhise V.D. Automotive Product Development: A Systems Engineering Implementation. Boca Raton, FL: CRC Press, 2017. ISBN: 9781498751270.
- [2] Ersoy M., Elbers C., and Schick B. "Fahrwerkentwicklung". In: Fahrwerkendbuch. Ed. by M. Ersoy and S. Gies. Wiesbaden: ATZ/MTZ Fachbuch, Springer Vieweg, 2017.
- [3] Abel H., Prokop G., Clauß R., and Wagner A. "Development of an axle design process for the chassis design within the early development stage". In: Apr. 2017, pp. 931–943. ISBN: 978-3-658-16987-9. DOI: 10.1007/978-3-658-16988-6\_73.
- [4] Abel H., Clauß R., Wagner A., and Prokop G. "Analytical extension of the effective axle characteristics concept for the development of a structured chassis design process". In: Vehicle System Dynamics 55.9 (2017), pp. 1297–1320. DOI: 10.1080/00423114.2017.1309055. URL: https://doi.org/10.1080/00423114.2017.1309055.
- [5] Abel H., Clauß R., Wagner A., and Prokop G. "Chassis Development in the Early Stage Using Analytical Target Cascading Methods". In: 25. Aachener Kolloquium Fahrzeug- und Motorentechnik. 2016.
- [6] Abel H. Entwicklung einer Fahrwerkauslegungsmethode für Pkw zur Anwendung in der Konzeptphase. Vol. Band 11. Schriftenreihe des Lehrstuhls Kraftfahrzeugtechnik. Göttingen: Cuvillier Verlag, 2019. ISBN: 978-3-7369-7114-1.

- [7] Reddy K.V., Madhu K., K. Chatra, and S. Bandyopadhyay. "A comprehensive kinematic analysis of the double wishbone and MacPherson strut suspension systems". In: *Mechanism and Machine Theory* 105 (2016), pp. 441–470. DOI: 10.1016/j.mechmachtheory.2016.07.017. URL: https://www.researchgate.net/publication/305824456\_A\_comprehensive\_kinematic\_analysis\_of\_the\_double\_wishbone\_and\_MacPherson\_strut\_suspension\_systems.
- [8] Hwang J.S., Kim S.R., and Han S.Y. "Kinematic Design of a Double Wishbone Type Front Suspension Mechanism Using Multi-Objective Optimization". In: *Proceedings of the 5th Australasian Congress on Applied Mechanics (ACAM)*. Brisbane, Australia, 2007, pp. 788–793. URL: https://espace.library.uq.edu.au/view/UQ:132197.
- [9] Sancibrián R., García P., et al. "Kinematic Design of Double-Wishbone Suspension Systems Using a Multiobjective Optimisation Approach". In: Vehicle System Dynamics 48.7 (2010), pp. 793-813. DOI: 10.1080/00423110903156574. URL: https://www.tandfonline.com/doi/abs/ 10.1080/00423110903156574.
- [10] Attia H.A. "Numerical Kinematic Analysis of the Standard MacPherson Motor-Vehicle Suspension System". In: KSME International Journal 17.12 (2003), pp. 1961–1968. DOI: 10.1007/BF02982435. URL: https://link.springer.com/article/10.1007/BF02982435.
- [11] Simionescu P.A. and Beale D. "Synthesis and Analysis of the Five-Link Rear Suspension System Used in Automobiles". In: *Mechanism and Machine Theory* 37.9 (2002), pp. 815–832. DOI: 10.1016/S0094-114X(02) 00037-X. URL: https://doi.org/10.1016/S0094-114X(02)00037-X.
- [12] Pedersen K., Bailey R., Allen J.K., and Mistree F. "Validating design methods & research: the validation square". In: ASME Design Engineering Technical Conferences. Baltimore, Maryland, USA, 2000, pp. 1–12.
- [13] Azmat Z. and Siddiqui M.A. "Analyzing Project Complexity, Its Dimensions and Their Impact on Project Success". In: Systems 11.8 (2023), p. 417. DOI: 10.3390/systems11080417. URL: https://doi.org/10.3390/systems11080417.

- [14] Fordand G., Gosling J., Naim M., and Syntetos A. "Simplifying complexity? On quality decision-making and non-conformance outcomes of megaprojects". In: *IEEE Transactions on Engineering Management* 71 (2024), pp. 5443–5454. DOI: 10.1109/TEM.2024.3359821.
- [15] Volvo Car Corporation. Overview Chassis Concept. Internal Resource. 2022.
- [16] Volvo Car Corporation. Volvo Concept Recharge. https://www.media. volvocars.com. n.d.
- [17] Wahde M. Biologically Inspired Optimization Methods. English. Southampton, UK: WIT Press, 2008. ISBN: 9781845641481. URL: https://worldcat.org/title/213448558.
- [18] Bottou L., Curtis F., and Nocedal J. "Optimization Methods for Large-Scale Machine Learning". In: SIAM Review 60.2 (2018), pp. 223–311. DOI: 10.1137/16M1080173.
- [19] Noda J. and Yu Q. "Study on design support method considering the interaction among multi-variables". In: *Proceedings of IMECE2008*. October 31-November 6, 2008. Boston, Massachusetts, USA, 2008.
- [20] Rumelhart D.E., Hinton G.E., and Williams R.J. "Learning representations by back-propagating errors". In: *Nature* 323.6088 (1986), pp. 533–536. DOI: 10.1038/323533a0. URL: https://doi.org/10.1038/323533a0.
- [21] Hinton G.E., Osindero S., and Teh Y. "A Fast Learning Algorithm for Deep Belief Nets". In: Neural Computation 18.7 (2006), pp. 1527-1554. DOI: 10.1162/neco.2006.18.7.1527. URL: https://doi.org/10. 1162/neco.2006.18.7.1527.
- [22] Mnih V., Kavukcuoglu K., et al. "Human-level control through deep reinforcement learning". In: Nature 518.7540 (Feb. 2015), pp. 529-533. ISSN: 1476-4687. DOI: 10.1038/nature14236. URL: https://doi.org/ 10.1038/nature14236.
- [23] Matschinsky W. Radführungen der Straßenfahrzeuge: Kinematik, Elasto-Kinematik und Konstruktion. 3rd ed. Berlin, Heidelberg, New York: Springer, 2007.

- [24] Albers I. "Erstellung eines Berechnungstools zur starrkinematischen Analyse von Einzelradaufhängungen". Diplomarbeit. Aachen: Rheinisch-Westfälische Technische Hochschule Aachen, 2003.
- [25] Hazem A.A. "Numerical Kinematic Analysis of the Standard Macpherson Motor-Vehicle Suspension System". In: *KSME International Journal* 17.12 (2003), pp. 1961–1968.
- [26] Heo J.H., Lee U.K., and Lee S.H. "Development of a Method to Compute the Kingpin Axis Using Screw Axis Theory Based on Suspension-Parameter Measuring Device Data". In: Journal of Automobile Engineering (2009). DOI: 10.1243/09544070JAUT01004.
- [27] Lee J.K. and Shim J.K. "Validity and Limitations of the Kinematic Roll Center Concept from the Viewpoint of Spatial Kinematics Using Screw Theory". In: *International Journal of Automotive Technology* 12.5 (2011), pp. 769–775.
- [28] Sommer III H. J. "Determination of First and Second Order Instant Screw Parameters from Landmark Trajectories". In: Journal of Mechanical Design (1992).
- [29] Bhat A.B. and Naik A. Suspension Steady-State Kinematics and Compliance Analysis Based On Linear Bushing Model. Master's thesis. 2020. URL: https://odr.chalmers.se/items/21cef337-9d8c-49f0-a0b0-e8fcda593663.
- [30] Kang J.S., Yun J.R., Lee J.M., and Tak T.O. "Elastokinematic Analysis and Optimization of Suspension Compliance Characteristics". In: *SAE Transactions* 106.5 (1997), pp. 87–93. DOI: 10.4271/970104.
- [31] Knapczyk J. and Dzierżek S. "Displacement and Force Analysis of Five-Rod Suspension with Flexible Joints". In: *Journal of Mechanical Design* 117.4 (1995), pp. 532–538. DOI: 10.1115/1.2836692.
- [32] Luedeke T.F., Köhler C., Conrad J., et al. "CPM/PDD as an integrated product and process model for a design-thinking based, agile product development process". In: *Proceedings of the DESIGN 2018 15th International Design Conference*. Ed. by D. Marjanović, M. Štorga, et al. DESIGN. 2018, pp. 2063–2074. DOI: 10.21278/idc.2018.0311. URL: https://doi.org/10.21278/idc.2018.0311.

- [33] Heo J.H., Lee U.K., and Lee S.H. "Development of a Method to Compute the Kingpin Axis Using Screw Axis Theory Based on Suspension-Parameter Measuring Device Data". In: *Proceedings of the Institution of Mechanical Engineers, Part D: Journal of Automobile Engineering* 223.4 (2009), pp. 519–531. DOI: 10.1243/09544070JAUT01004. URL: https://journals.sagepub.com/doi/10.1243/09544070JAUT01004.
- [34] Lee J.K. and Shim J.K. "Validity and Limitations of the Kinematic Roll Center Concept from the Viewpoint of Spatial Kinematics Using Screw Theory". In: *International Journal of Automotive Technology* 12.5 (2011), pp. 769–775. DOI: 10.1007/s12239-011-0089-6. URL: https://link.springer.com/article/10.1007/s12239-011-0089-6.
- [35] Rocca E. and Russo R. "A Feasibility Study on Elastokinematic Parameter Identification for a Multilink Suspension". In: Proceedings of the Institution of Mechanical Engineers, Part D: Journal of Automobile Engineering 216.2 (2002), pp. 153–160. DOI: 10.1243/0954407021528995. URL: https://journals.sagepub.com/doi/10.1243/0954407021528995.
- [36] Knapczyk J. and Dzierżek S. "Displacement and Force Analysis of Five-Rod Suspension with Flexible Joints". In: *Journal of Mechanical Design* 117.4 (Dec. 1995), pp. 532-538. DOI: 10.1115/1.2826720. URL: https://asmedigitalcollection.asme.org/mechanicaldesign/article/117/4/532/425732/Displacement-and-Force-Analysis-of-Five-Rod.
- [37] Tang L., Wen-Bin S., and Dai L. "A Calculation Method of Joint Forces for a Suspension Considering Nonlinear Elasticity of Bushings". In: *Proceedings of the Institution of Mechanical Engineers, Part K: Journal of Multibody Dynamics* (2012). DOI: 10.1177/1464419312452214. URL: https://journals.sagepub.com/doi/10.1177/1464419312452214.
- [38] Kang J.S., Yun J.R., Lee J.M., and Tak T.O. Elastokinematic Analysis and Optimization of Suspension Compliance Characteristics. Tech. rep. 970104. SAE International, 1997. DOI: 10.4271/970104. URL: https://doi.org/10.4271/970104.
- [39] Caputo A., Spina M., and Guglielmino E. "Sensitivity of Suspension System Performance to Bushing Stiffness Variation An Evaluation Methodology". In: *SAE Transactions* 112 (2003), pp. 166–177. DOI:

- 10.4271/2003-01-0237. URL: https://doi.org/10.4271/2003-01-0237.
- [40] Williams R.J. "Simple Statistical Gradient-Following Algorithms for Connectionist Reinforcement Learning". In: *Machine Learning* 8.3-4 (1992), pp. 229–256. DOI: 10.1007/BF00992696. URL: https://doi.org/10. 1007/BF00992696.
- [41] Crăciun I. and Ungureanu M. "On jerk in the kinematic study of the rigid body". In: *IOP Conference Series: Materials Science and Engineering* 749.1 (2020), p. 012004. DOI: 10.1088/1757-899X/749/1/012004.
- [42] Huang Y. "Knowledge & Requirements Based Wheel Suspension Template". Master's Thesis. Stuttgart, Germany: Institut für Verbrennungsmotoren und Kraftfahrwesen, Universität Stuttgart, 2018.
- [43] Huang Y. "Target-driven Road Vehicle Suspension Design". Licentiate thesis. Gothenburg, Sweden: Chalmers University of Technology, 2022. URL: https://research.chalmers.se/en/publication/533119.
- [44] VI-grade. VI-CarRealTime. https://www.vi-grade.com/en/products/vi-carrealtime. Version 2024.2. 2024.
- [45] Brockman G., Cheung V., Pettersson L., Schneider J., et al. OpenAI Gym. https://arxiv.org/abs/1606.01540. 2016.
- [46] Sutton R.S. and Barto A.G. Reinforcement Learning: An Introduction. Cambridge, MA, USA: A Bradford Book, 2018. ISBN: 0262039249.
- [47] Paszke A., Gross S., Massa F., Lerer A., et al. "PyTorch: An imperative style, high-performance deep learning library". In: *Advances in Neural Information Processing Systems*. Vol. 32, 2019, pp. 8024–8035.
- [48] Sutton R.S. "Learning to predict by the methods of temporal differences". In: *Machine Learning* 3.1 (1988), pp. 9–44. DOI: 10.1007/BF00115009.